

**STUDY OF DIELECTRIC RESPONSE OF BISMUTH  
FERRITE-BASED MATERIALS UNDER LIGHT  
IRRADIATION**



**A Thesis Submitted in Partial Fulfillment of the Requirements for the  
Degree of Master of Science in Physics  
Suranaree University of Technology  
Academic Year 2016**

การศึกษาการตอบสนองไดอิเล็กทริกของวัสดุกลุ่มบิสมัทเฟรไรต์ภายใต้  
เงื่อนไขการฉายแสง



วิทยานิพนธ์นี้เป็นส่วนหนึ่งของการศึกษาตามหลักสูตรปริญญาวิทยาศาสตรมหาบัณฑิต  
สาขาวิชาฟิสิกส์  
มหาวิทยาลัยเทคโนโลยีสุรนารี  
ปีการศึกษา 2559

**STUDY OF DIELECTRIC RESPONSE OF BISMUTH FERRITE-  
BASED MATERIALS UNDER LIGHT IRRADIATION**

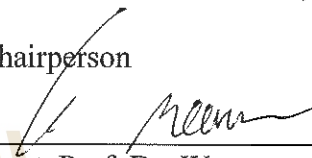
Suranaree University of Technology has approved this thesis submitted in partial fulfillment of the requirements for a Master's Degree.

Thesis Examining Committee



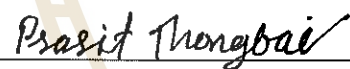
(Prof. Dr. Santi Maensiri)

Chairperson



(Asst. Prof. Dr. Worawat Meevasana)

Member (Thesis Advisor)



(Asst. Prof. Dr. Prasit Thongbai)

Member



(Assoc. Prof. Dr. Prayoon Songsiririthigul)

Member



(Assoc. Prof. Dr. Rattikorn Yimnirun)

Member



(Prof. Dr. Sukit Limpijumnong)

Vice Rector for Academic Affairs  
and Innovation



(Prof. Dr. Santi Maensiri)

Dean of Institute of Science

ศราวฤดี นาถาบำรุง : การศึกษาการตอบสนองไดอิเล็กทริกของวัสดุกลุ่มบิสมัทเฟอร์ไรต์ ภายใต้เงื่อนไขการฉายแสง (STUDY OF DIELECTRIC RESPONSE OF BISMUTH FERRITE-BASED MATERIALS UNDER LIGHT IRRADIATION).

อาจารย์ที่ปรึกษา : ผู้ช่วยศาสตราจารย์ ดร.วรวัดน์ มีวาสนา, 67 หน้า.

งานวิทยานิพนธ์นี้สนใจศึกษาสมบัติของ  $\text{Bi}_{1-x}\text{M}_x\text{FeO}_3$  ที่มีสารละลายของแข็ง M คือ La และ Ba ที่ความเข้มข้น  $x = 0, 0.05, 0.1, 0.2$  และ  $0.3$  ซึ่งมีสมบัติแม่เหล็กเฟอร์โรอิกและมีค่าไดอิเล็กทริกที่สูงอยู่ในช่วงหลักหมื่นที่อุณหภูมิห้อง โดยในงานวิจัยนี้ได้พบว่าภายใต้การฉายแสงเลเซอร์สีม่วงและสีเขียว (ความยาวคลื่น 405 นาโนเมตร และ 523 นาโนเมตร ตามลำดับ) บนตัวเก็บประจุที่ใช้ BLFO ( $x = 0.1$ ) เป็นสารไดอิเล็กทริกจะมีการเพิ่มขึ้นของค่าความเก็บประจุไฟฟ้าได้ถึง 12 เปอร์เซ็นต์ และ 10 เปอร์เซ็นต์ ตามลำดับ จากค่าความจุเริ่มต้นประมาณ 620 พิโคฟารัด ซึ่งวัดที่ความถี่ 1 กิโลเฮิร์ตซ์ โดยสาร BFO ที่ค่าความถี่อื่น ๆ ก็แสดงการเพิ่มของค่าความจุที่ต่างกันไปตามรายละเอียดด้านใน

เพื่อทราบที่มาของการเพิ่มค่าความจุนี้ได้ทำการศึกษาโครงสร้างอิเล็กทรอนิกส์ของสารตัวอย่างด้วยเทคนิคโฟโตมิชชันสเปกโทรสโกปี และวัดสภาพความต้านทานที่เปลี่ยนไปภายใต้การฉายแสง ซึ่งพบว่าภายใต้การฉายแสงบนผิวหน้าสารจะชักจูงให้เกิดช่องว่างของออกซิเจน แล้วอาจนำไปสู่การมีโครงสร้างอิเล็กทรอนิกส์ในแบบ 2 มิติบนผิวหน้า ซึ่งสอดคล้องกับค่าความต้านทานของสารซึ่งลดลงได้ภายใต้การฉายแสง ในแบบจำลองการเกิดโครงสร้างอิเล็กทรอนิกส์ 2 มิตินี้จะทำให้เสมือนว่ามีตัวเก็บประจุเชิงควอนตัมเพิ่มอีกตัวที่มาต่ออนุกรมกับสารตั้งต้น โดยถ้าค่าความจุควอนตัมนี้มีค่าติดลบในกรณีที่สารมีสภาพการบีบอัดอิเล็กตรอนเชิงลบจะทำให้มีค่าความจุไฟฟ้ารวมมีค่าเพิ่มขึ้น และจากการทดลองวัดด้วยเทคนิคโฟโตมิชชันสเปกโทรสโกปีพบว่า  $\text{Bi}_{0.95}\text{La}_{0.05}\text{FeO}_3$  แสดงสมบัติการบีบอัดอิเล็กตรอนเชิงลบโดยสังเกตได้จากการลดลงของค่าพลังงานศักย์ไฟฟ้าเมื่อมีการเติมอิเล็กตรอนเข้าสู่ผิวหน้าของสารในขณะที่ฉายแสง โดยการที่แสงเข้ากระตุ้นอะตอมของออกซิเจนให้หลุดออกจากผิวหน้าและออกซิเจนที่หลุดไปนี้ได้ทิ้งอิเล็กตรอนไว้บนผิวหน้าของก้อนสาร ผลการทดลองนี้สอดคล้องกับการเพิ่มขึ้นของค่าความจุไฟฟ้าภายใต้การฉายแสงข้างต้น ความรู้ที่ได้จากการศึกษานี้จะทำให้เราสามารถนำประโยชน์จากสมบัติเชิงควอนตัมของอิเล็กตรอนที่อยู่สภาพ 2 มิติซึ่งแตกต่างจากสมบัติเชิงก้อนของสาร เพื่อใช้ในการออกแบบอุปกรณ์อิเล็กทรอนิกส์แบบใหม่ ๆ รวมถึงเซนเซอร์ และระบบกักเก็บพลังงานที่มีประสิทธิภาพสูง

สาขาวิชาฟิสิกส์  
ปีการศึกษา 2559

ลายมือชื่อนักศึกษา   
ลายมือชื่ออาจารย์ที่ปรึกษา 

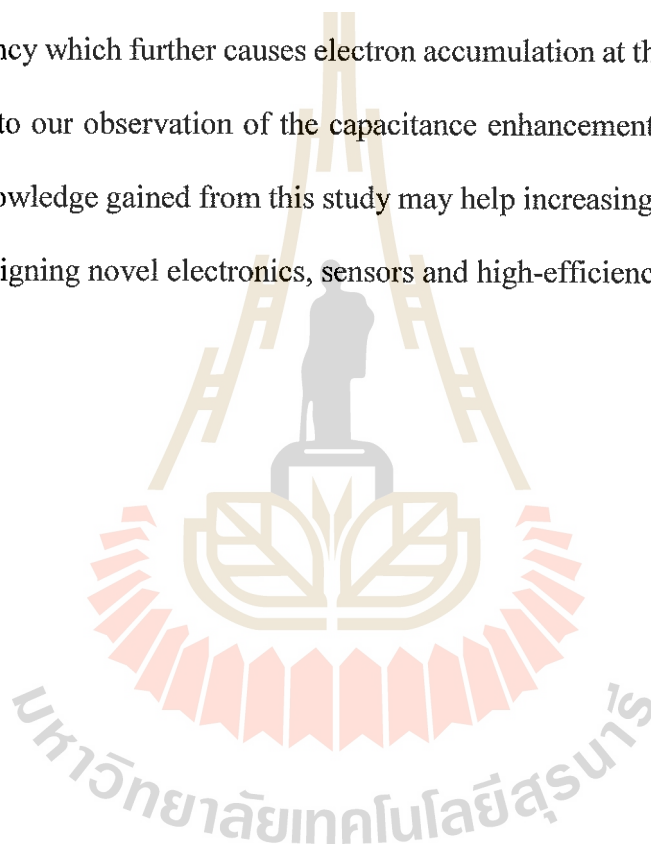
SARAWUDH NATHABUMROONG : STUDY OF DIELECTRIC  
RESPONSE OF BISMUTH FERRITE-BASED MATERIALS UNDER  
LIGHT IRRADIATION. THESIS ADVISOR : ASST. PROF. WORAWAT  
MEEVASANA, Ph.D. 67 PP.

BISMUTH FERRITE/PHOTOEMISSION SPECTROSCOPY/NEGATIVE  
ELECTRON COMPRESSIBILITY/ELECTRONIC STRUCTURE/CAPACITANCE  
ENHANCEMENT

In this thesis work, we are interested in studying the properties of  $\text{Bi}_{1-x}\text{M}_x\text{FeO}_3$  where  $\text{M} = \text{La}$  and  $\text{Ba}$  and  $x = 0, 0.05, 0.1, 0.2$  and  $0.3$ . This bismuth ferrite  $\text{BiFeO}_3$  (BFO) has multiferroic property and high dielectric in the order of  $10^4$  at room temperature. In this work, it was observed that, the capacitor with  $\text{Bi}_{1-x}\text{La}_x\text{FeO}_3$  ( $x = 0.1$ ) as dielectric material could have higher electrical capacitance up to 10% and 12% under irradiation of green and violet laser (wavelength of 532 nm and 405 nm, respectively) where the original capacitance was 620 pF and the measuring frequency was 1 kHz. For other dopings, similar enhancements were also observed with details later described in the thesis.

To investigate the origin of this enhancement effect, we studied the electronic structure of these BFO materials were studied by using photoemission spectroscopy (PES). The change in resistance under irradiation was also measured. It was found that the irradiation could cause the oxygen vacancy at the surface which might lead to the formation of two-dimensional electron gas (2DEG) at the surface. This agrees with the observation of the clear reduction in resistance upon increasing irradiation dose. From the model of this 2DEG formation, it is expected that this 2DEG layer will act like an

additional quantum capacitor connecting with the original capacitor in series. If this quantum capacitance is negative in the case that the material exhibits the so called negative electron compressibility (NEC), the total capacitance will be enhanced. By using PES, it was found that our BFO samples exhibited this NEC effect where the measured chemical potential became lower upon increasing the electron density (induced by laser/synchrotron irradiation). This laser/synchrotron irradiation can induce oxygen vacancy which further causes electron accumulation at the sample surface. This corresponds to our observation of the capacitance enhancement upon irradiation very well. The knowledge gained from this study may help increasing the usage of this NEC effect for designing novel electronics, sensors and high-efficiency energy storage.



School of Physics

Academic Year 2016

Student's Signature

Advisor's Signature


## ACKNOWLEDGEMENTS

My thesis could not be accomplished without help and support from many people. First of all, I would like to thank my advisor, Asst. Prof. Dr. Worawat Meevasana. Before, I graduated with a bachelor's degree and I had chance to talk with him for researching about synchrotron that made me decided to join this research group. He is very nice advisor, kind, dedicated. He gave chances to me for research in Italy (Electra synchrotron) and United State of America (ALS) that gave very valuable experience to me. Since I joined in this group, he helps me to develop myself, push me to have better attitude for research and made me better.

I would like to thank Asst. Prof. Dr. Prasit Thongbai, who is my kind advisor of undergraduate research project at Khon Kaen University. He has important hand to help me for graduating in bachelor's degree and suggested me to join with Asst. Prof. Dr. Worawat Meevasana.

I would like to acknowledge Prof. Dr. Santi Maensiri, Assoc. Prof. Dr. Prayoon Songsiririthigul and Assoc. Prof. Dr. Rattikorn Yimmirun, thesis defense committee, for giving their valuable time and guiding good research aspects for my thesis defense and also give me many advices to make me better.

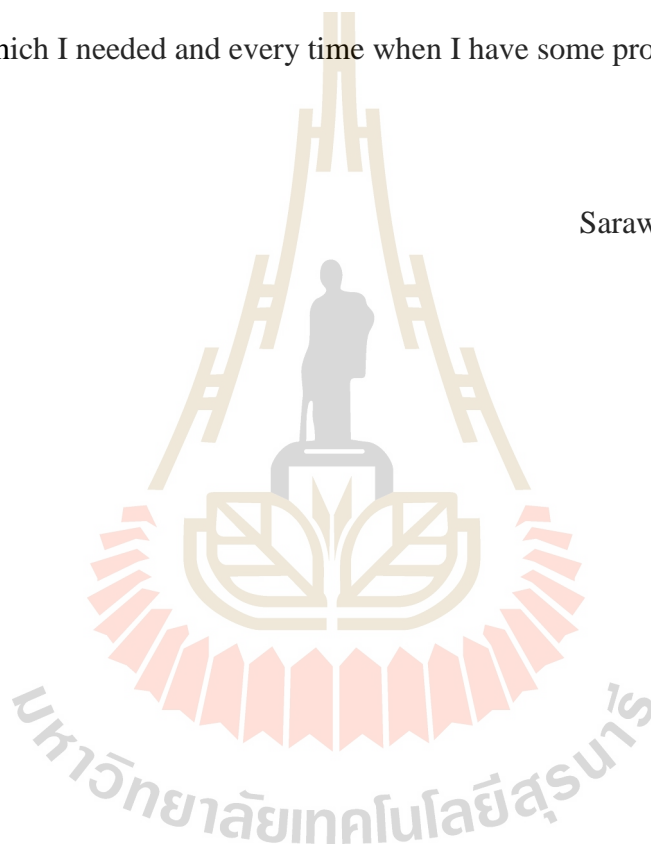
I am thankful to every persons at Beamline 3.2 at Synchrotron Light Research Institute (SLRI), Dr. Hideki Nakajima, Mr. Surachet, Dr. Ratchadaporn and Mr. Thanit for help in PES measurements.

I would like to thank Miss Benjaporn Yotburut for preparing samples which were measured in this research.

I would like to acknowledge my scholarship which is the Science Achievement Scholarship of Thailand (SAST) for financial support since bachelor's degree.

And finally, I want to give big thank to every people in Meevasana group, my family, all teachers, all staffs and students in School of Physics for supporting me to everything which I needed and every time when I have some problems.

Sarawudh Nathabumroong



# CONTENTS

	<b>Page</b>
ABSTRACT IN THAI .....	I
ABSTRACT IN ENGLISH .....	II
ACKNOWLEDGEMENTS .....	IV
CONTENTS .....	VI
LIST OF FIGURES .....	IX
<b>CHAPTER</b>	
<b>I INTRODUCTION</b> .....	<b>1</b>
1.1 Background and significance of the study .....	1
1.2 Objectives .....	2
<b>II REVIEW OF THE LITERATURE</b> .....	<b>4</b>
2.1 Electrical and magnetic properties of BiFeO <sub>3</sub> .....	4
2.2 Capacitance enhancement under UV irradiation and negative electron compressibility .....	13
<b>III METHODOLOGY AND MEASUREMENT</b> .....	<b>19</b>
3.1 Sample growth/ Samples preparation .....	19
3.2 Impedance analyzer measurement .....	22
3.2.1 Impedance analyzer .....	23
3.2.2 Fixture .....	24
3.2.3 Capacitance .....	24

## CONTENT (Continued)

	<b>Page</b>
3.2.4 Quality factor .....	26
3.2.5 Loss tangent .....	27
3.3 Photoemission spectroscopy .....	28
3.3.1 Photon energy .....	30
3.3.2 Zeroth order light .....	30
3.3.3 Photoelectric effect .....	31
3.3.4 Principles of photoemission spectroscopy .....	32
3.3.5 Oxygen vacancy .....	33
3.3.6 Method to check the effect of negative electron compressibility .....	33
<b>IV RESULTS AND DISCUSSION</b> .....	<b>37</b>
4.1 Dielectric measurement of bismuth ferrite-based materials by impedance analyzer .....	37
4.1.1. Bismuth ferrite ( $\text{BiFeO}_3$ ) .....	37
4.1.2. BBFO-0.05 ( $\text{Bi}_{0.95}\text{Ba}_{0.05}\text{FeO}_3$ ) .....	39
4.1.3. BBFO-0.1 ( $\text{Bi}_{0.9}\text{Ba}_{0.1}\text{FeO}_3$ ) .....	41
4.1.4. BBFO-0.2 ( $\text{Bi}_{0.8}\text{Ba}_{0.2}\text{FeO}_3$ ) .....	42
4.1.5. BBFO-0.3 ( $\text{Bi}_{0.7}\text{Ba}_{0.3}\text{FeO}_3$ ) .....	43
4.1.6. BLFO-0.05 ( $\text{Bi}_{0.95}\text{La}_{0.05}\text{FeO}_3$ ) .....	44
4.1.7. BLFO-0.1 ( $\text{Bi}_{0.9}\text{La}_{0.1}\text{FeO}_3$ ) .....	46
4.1.8. BLFO-0.2 ( $\text{Bi}_{0.8}\text{La}_{0.2}\text{FeO}_3$ ) .....	47

## CONTENT (Continued)

	<b>Page</b>
4.1.9. BLFO-0.3 ( $\text{Bi}_{0.7}\text{La}_{0.3}\text{FeO}_3$ ) .....	48
4.1.10. Resistance measurement under irradiation .....	49
4.2 Photoemission measurement and signatures of negative electron compressibility .....	51
4.2.1 $\text{BiFeO}_3$ .....	51
4.2.2 BLFO-0.05 .....	52
4.2.3 BBFO-0.05.....	54
4.3 Discussions and calculation of capacitance enhanced by the negative electron compressibility effect.....	55
<b>V CONCLUSIONS AND FUTURE RESEARCH .....</b>	<b>58</b>
5.1 Conclusions.....	58
5.2 Improvement/ future plan .....	59
REFERENCES.....	60
CURRICULUM VITAE.....	67

## LIST OF FIGURES

Figure	Page
2.1 Atomic structure of bismuth ferrite ( $\text{BiFeO}_3$ ).....	5
2.2 The schematic diagram shows IBLC structure.....	6
2.3 Assume IBLC structure inside bismuth ferrite-base materials sample.....	6
2.4 Applied voltage on sample between two electrodes.....	7
2.5 Inside electric field in grain.....	7
2.6 (a) XANES spectra of $\text{Bi}_{1-x}\text{La}_x\text{FeO}$ powders, (b) TEM image of BLFO-0.05.....	9
2.7 XRD patterns of powders calcined at $600^\circ\text{C}$ (a) for 3 hours and ceramics sintered at $800^\circ\text{C}$ for 3 hours (b).....	9
2.8 Trend of all BBFO-X ( $x = 0.05, 0.1, 0.2, 0.3$ ) loss tangents with various frequency.....	10
2.9 Trend of all BLFO-X ( $x = 0, 0.05, 0.1, 0.2, 0.3$ ) loss tangents with various frequency.....	11
2.10 Capacitance and loss tangent of CCTO at 1000 Hz.....	14
2.11 Photoemission spectroscopy of CCTO at Advance Light - Source (ALS).....	15
2.12 The time dependence of resistance of CCTO upon exposure to light at SLRI....	16
3.1 (a) SEM picture of $\text{BiFeO}_3$ and (b) SEM picture of BLFO-0.05.....	20
3.2 Bismuth ferrite-based materials.....	21
3.3 Tool for determining thickness of samples.....	21

## LIST OF FIGURES (Continued)

Figure	Page
3.4 Polishing equipment (a), diamond jell (b) .....	22
3.5 Schematic diagram of capacitance and loss tangent measurements .....	23
3.6 Front view (a) and top view (b) of fixture .....	24
3.7 Diagram of bismuth ferrite-based materials same as capacitor .....	25
3.8 Diagram in bismuth ferrite-based materials when we ignore inductive part .....	25
3.9 Diagram in bismuth ferrite-based materials when we consider Impedance .....	26
3.10 Flow chart of conditions of measurement in this research .....	30
3.11 Mechanism of photoelectric effect .....	31
3.12 Mechanism of photoelectric effect photoemission spectroscopy .....	32
3.13 The simplified models for the possible mechanisms of oxygen-vacancy formation.....	33
3.14 Diagram of capacitance measurement .....	35
3.15 Electronic structure of (a) Fermi surface, (b) valence band versus doping .....	36
4.1 Capacitance and loss tangent of BiFeO <sub>3</sub> under green irradiation approximate 4.1 $\frac{W}{\text{cm}^2}$ (a-d), under violet irradiation approximate $1.8 \frac{W}{\text{cm}^2}$ (e-h) .....	38
4.2 Percentage change of capacitance and loss tangent under all conditions for BiFeO <sub>3</sub> .....	39

## LIST OF FIGURES (Continued)

Figure	Page
4.4 Percentage change of capacitance and loss tangent under all conditions for BBFO-0.05 .....	40
4.5 Percentage change of capacitance and loss tangent under all conditions for BBFO-0.1 .....	41
4.6 Percentage change of capacitance and loss tangent under all conditions for BBFO-0.2 .....	42
4.7 Percentage change of capacitance and loss tangent under all conditions for BBFO-0.3 .....	44
4.8 Capacitance and loss tangent of BLFO-0.05 under green irradiation approximate $4.1 \frac{W}{cm^2}$ (a-d), under violet irradiation approximate $1.8 \frac{W}{cm^2}$ (e-h) ...	45
4.9 Percentage change of capacitance and loss tangent under all conditions for BLFO-0.05 .....	46
4.10 Percentage change of capacitance and loss tangent under all conditions for BLFO-0.1 .....	47
4.11 Percentage change of capacitance and loss tangent under all conditions for BLFO-0.2 .....	48
4.12 Percentage change of capacitance and loss tangent under all conditions for BLFO-0.3 .....	49
4.13 Resistance of BLFO-0.05 under green irradiation about $4.1 \frac{W}{cm^2}$ (a) and under violet irradiation about $1.7 \frac{W}{cm^2}$ (b).....	50

## LIST OF FIGURES (Continued)

Figure	Page
4.14 Spectra of valance band of thin film bismuth ferrite .....	52
4.15 (a) Spectra of valance bands of BLFO-0.05. (b) energy shift of VB vs irradiation time .....	52
4.16 Spectra of valance band of BLFO-0.05 .....	53
4.17 Spectra of valance bands of BBFO-0.05 .....	54
4.18 Relationships between $C_{Total}$ from real measurement (a), $C_{Total}$ From calculation (b) with total dos.....	57

# CHAPTER I

## INTRODUCTION

### 1.1 Background and significance of the study

For a long time, many materials in bulk form have been investigated by various methods so that unique/useful properties can be revealed. For the past few decades, scientists have particularly been interested in materials with nano-scale structure or reduced-dimension structure (e.g. 2D materials in atomic structure or electronic structure). Graphene is one of the most famous materials with two-dimensional atomic structure which shows many exotic properties including ultra-high mobility, high thermal conductivity, transparency, and quantum Hall effect. On the other hand, there could also be materials in bulk form which could show two-dimensional electronic structure; one example is two-dimensional electron gas (2DEG) at oxide surface which could exhibit many properties which may not be available in bulk materials. To study 2D materials, photoemission spectroscopy (PES) is one among accessible techniques which uses light for measuring their electronic structure (e.g. study of WSe<sub>2</sub> (Riley et al., 2015)). At the same time, this light (or irradiation) can also create 2DEG at the surfaces of certain oxides e.g. SrTiO<sub>3</sub> (Meevasana et al., 2011). This irradiation can also affect other electronic properties; for an example, it was reported that the capacitance with CaCu<sub>3</sub>Ti<sub>4</sub>O<sub>12</sub> (CCTO) as the dielectric material can increase under violet irradiation (Masingboon et al., 2013); although it was directly proven, the data suggest that the effect might be caused by the nature of 2D electronic structure.

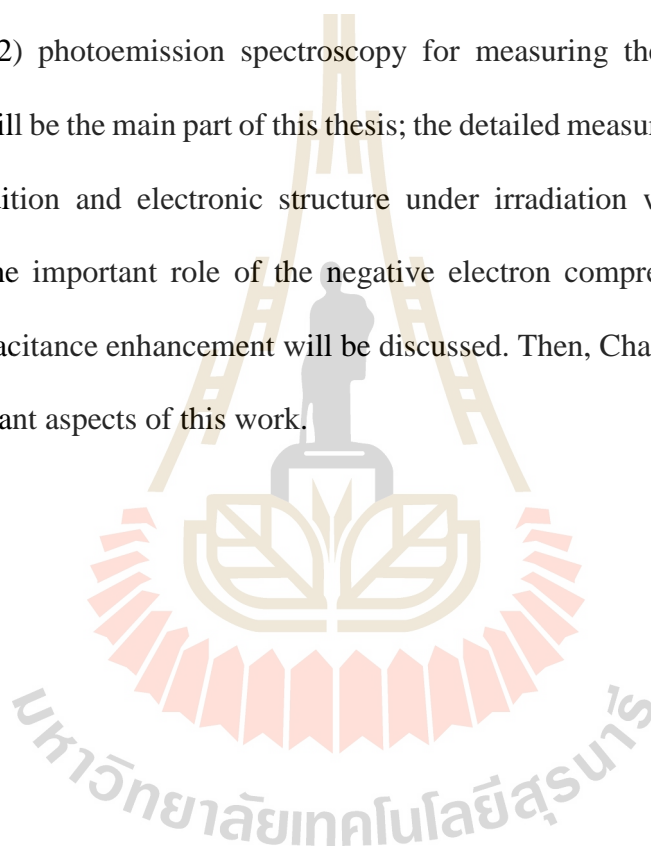
At our university, many oxide materials prepared by various techniques are available through collaboration for further studies; among these, bismuth ferrite-based materials prepared by co-precipitation method in Prof. Santi Maensiri's group (Yotburut et al., 2014) are interesting to us because they exhibit multiferroic property, displaying both ferroelectricity with Curie temperature ( $T_C$ ) of 1103 K and antiferromagnetism with Neel temperature ( $T_N$ ) of 643 K (Wang et al., 2003). Regarding their dielectric property, these materials also exhibit high dielectric and low loss tangent. This motivated us to further study the irradiation effect on its electrical capacitance, similar to the CCTO study. Indeed, we actually found that the effective dielectric of  $\text{BiFeO}_3$  materials could be enhanced under irradiation, similar to CCTO (as explained later). In this thesis, we try to focus on examining the origin of this effect through its electronic structure by using photoemission spectroscopy where our hypothesis centers around the nature of 2D electronic structure. The understanding of this nature may help increasing the potential usages of these oxides materials in applications including energy storage, sensors and other electronic devices.

## 1.2 Objectives and structure of this thesis

In this thesis, there are 3 objectives as the following:

1. To study capacitance and loss tangent of bismuth ferrite based materials under green and violet irradiation by using the fixture and impedance analyzer.
2. To investigate the electronic structure of bismuth ferrite based materials under UV irradiation using photoemission spectroscopy (PES).
3. To use the information of the measured electronic structure for understanding the origin of any changes of the capacitance under irradiation.

Based on these objectives, the next chapter (Chapter II) will start with the literature review of the basic properties of  $\text{BiFeO}_3$  and the effect so called “negative electron compressibility” which explains how electrical capacitance could be enhanced due to the nature of 2D electronic structure. Then, Chapter III will explain the various instrumental aspects of the experimental measurements used in this work; there are mainly 1) impedance analyzer used for measuring electrical capacitance and loss tangent and 2) photoemission spectroscopy for measuring the electronic structure. Chapter IV will be the main part of this thesis; the detailed measurements of capacitance in each condition and electronic structure under irradiation will be explained and discussed. The important role of the negative electron compressibility effect in the observed capacitance enhancement will be discussed. Then, Chapter V will summarize all the important aspects of this work.



## CHAPTER II

### REVIEW OF THE LITERATURE

#### 2.1 Electrical and magnetic properties of BiFeO<sub>3</sub>

In this research, we are interested in the famous bismuth ferrite-based materials (BiFeO<sub>3</sub> and doped- BiFeO<sub>3</sub>). Bismuth ferrite (BFO) is one of the most prominent multiferroic materials which exhibit more than one elementary ferroic order parameter simultaneously (where example has a single phase). However, definition of multiferroic can be expanded to non-primary ferroic order variables such ferromagnetism, ferroelectricity and so on. The single crystals of BiFeO<sub>3</sub> have been shown to have a rhombohedrally distorted perovskite structure (Figure 2.1) with lattice parameter ( $a = b = c = 0.563$  nm) and ( $\alpha = \beta = \gamma = 59.4^\circ$ ) (Wang et al., 2003). BiFeO<sub>3</sub> ceramics were also classified as rhombohedral with space group R3c but lattice parameter ( $a = 3.958$ , and  $\alpha = 89.30^\circ$ ) (Gheorghiu et al., 2013). BiFeO<sub>3</sub> exhibits ferroelectric Curie temperature ( $T_C$ ) of about 1103 K and is antiferromagnetic with Neel temperature ( $T_N$ ) of 643 K (Wang et al., 2003). Single-phased BiFeO<sub>3</sub> ceramic can be synthesized by using a rapid liquid phase sintering technique and ferroelectric hysteresis loops can be measured at room temperature (Wang et al., 2004). These properties attract much attention from many researchers around the world as they could potentially be used in electronic applications.

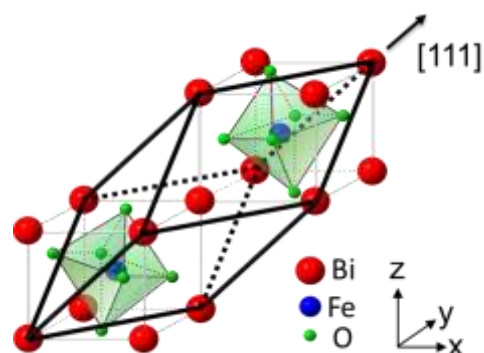


**Figure 2.1** Atomic structure of bismuth ferrite ( $\text{BiFeO}_3$ ) (picture from <http://www.intechopen.com/books/ferroelectrics-physical-effects/multifunctional-characteristics-of-b-site-substituted-bifeo3-films>).

The structure of ferroelectric phase was analyzed by using both x-ray and Neutron diffractions to be savvied distorted perovskite structure (Neaton et al., 2005). There is an antiferromagnetic spin ordering but also shows a soft ferromagnetic moment arising from a canted spin structure (Dho et al., 2006). In 2007,  $\text{BiFeO}_3$  was shown that the antiferromagnetic and ferroelectric orders coexist with very high transition temperatures ( $T_g$ ) (Lebeugle et al., 2007). This material exhibited weak magnetization of about  $0.02\mu_B/\text{Fe}$  in bulk. Then, the magnetic hysteresis loops exhibit exchange bias as well as asymmetry in vertical that causes spin pinning on around a boundaries between antiferromagnetic domains and ferromagnetic domains (Mazumder et al., 2007). Godara and his group reported the ferroelectric at Curie temperature  $T_C$  is 1,100 K and the antiferromagnetic at Neel temperature  $T_N$  is 640 K (Godara et al., 2014).

$\text{BiFeO}_3$  is also called a giant dielectric material because of its high dielectric constant and low loss tangent. The reason of high dielectric and low loss tangent was proposed to be due to internal barrier layer capacitor (IBLC) (Putjuso, 2012) as shown

in Figure 2.2. Opaque cubics represent grains which can collect electrical charge. Black line square is insulator which blocks electrical charge going out of its grains.

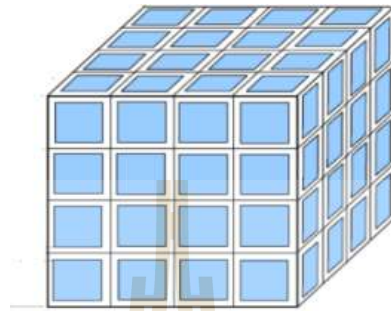


**Figure 2.2** The schematic diagram shows IBLC structure (Putjuso, 2012).

Figures 2.3- 2.5 below show mechanism when these materials were applied electric field. IBLC structure is assumed to have electrical charges distribute in grains. Edge of each grain are called grain boundary that are insulating. Therefore, electrical charges are confined in each grain interior sample as shown in Figure 2.3.

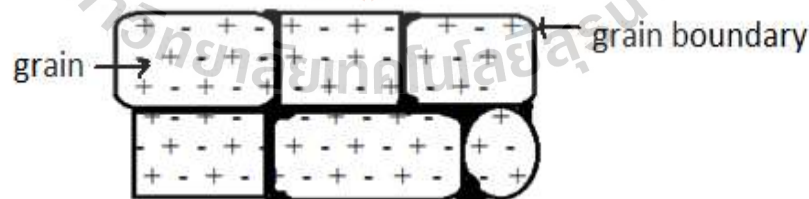


**Figure 2.3** Assumed IBLC structure inside bismuth ferrite-base materials sample.

Then, fixed voltage is applied between two electrodes. After that, these electrical charges will be induced by external electrical force. Then, they will be like array as shown in Figure 2.4.

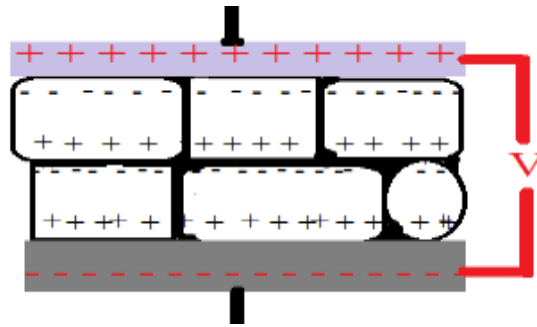


**Figure 2.4** Applied voltage on sample between two electrodes.

In each grain, electric field (blue arrow) will appear inside grains. That electric field is in opposite direction with external electric field (red arrow). That picture shows external electric field ( $E$ ) which will be decreased when structure of materials has more grains as shown in Figure 2.5.

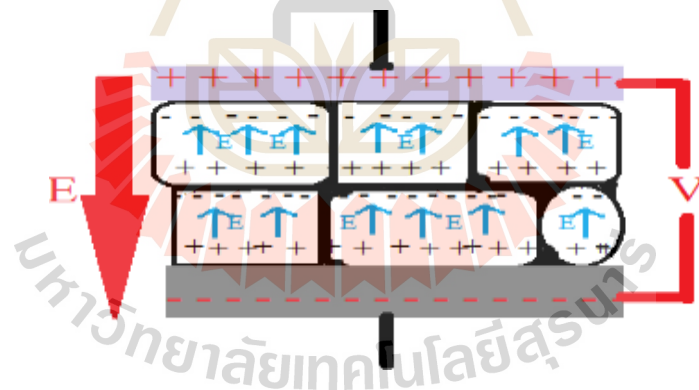


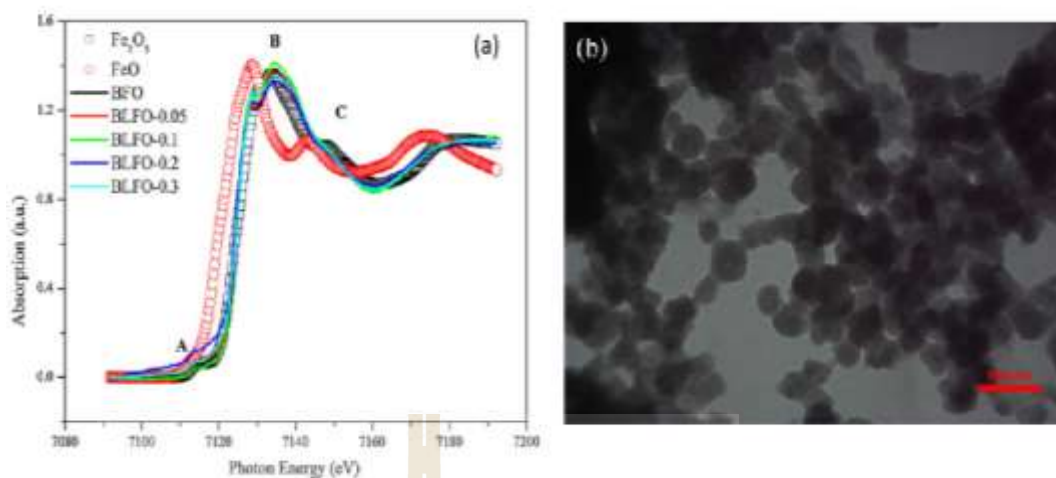
**Figure 2.5** Inside electric field in grain.

Therefore, capacitance of this sample will be increased as shown in below equation.

$$C = \frac{Q}{V} = \frac{Q}{ED - \sum E_{\text{inside}}d} \quad (1)$$

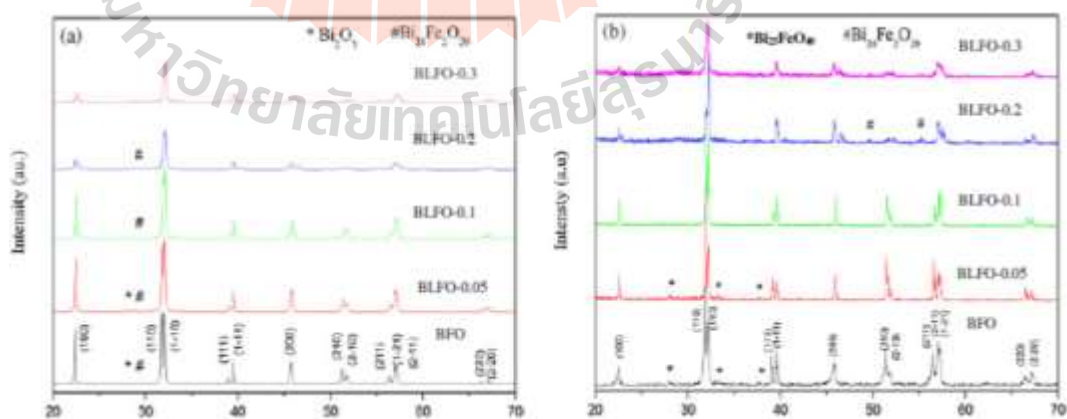
Where  $C$  is capacitance,  $Q$  is electrical charge,  $V$  is applied voltage,  $E$  is external electric field,  $D$  is distance between two electrodes,  $E_{\text{inside}}$  is internal electric field of each grain and  $d$  is distance between positive charges array and negative charges array inside each grain.

$\text{BiFeO}_3$  ceramics can be prepared by several methods such as so-gel method, precipitation method, and rapid liquid phase sintering technique etc. In this work, these bismuth ferrite-based materials were synthesized by using a simple coprecipitation method. They were prepared by Benjaporn Yotburut in Prof. Dr. Santi Maensiri's group. These samples exhibit higher dielectric value ( $\epsilon'$ ). Dielectric value of  $\text{Bi}_{1-x}\text{La}_x\text{FeO}_3$  is highest with optimal doping of  $x = 0.05$ . The doped  $\text{La}^{3+}$  will replace bismuth ( $\text{Bi}^{3+}$ ) in structure. This was confirmed by XANES spectra measured at beamline 5 of the Synchrotron Light Research Institute (SLRI), as shown in Figure 2.6(a). Dielectric relaxation behavior in these ceramic samples may be caused by the effect of  $\text{La}^{3+}$  ions on the formation and distribution of  $\text{Fe}^{2+}$  ions.  $\text{BiFeO}_3$  was measured by TEM technique. They found that morphology of powders is spherical and particle sizes were typically less than 100 nm as shown in Figure 2.6(b). They also found that particle size of  $\text{Bi}_{1-x}\text{La}_x\text{FeO}_3$  decreased with increasing quantitative La (Yotburut et al., 2014).



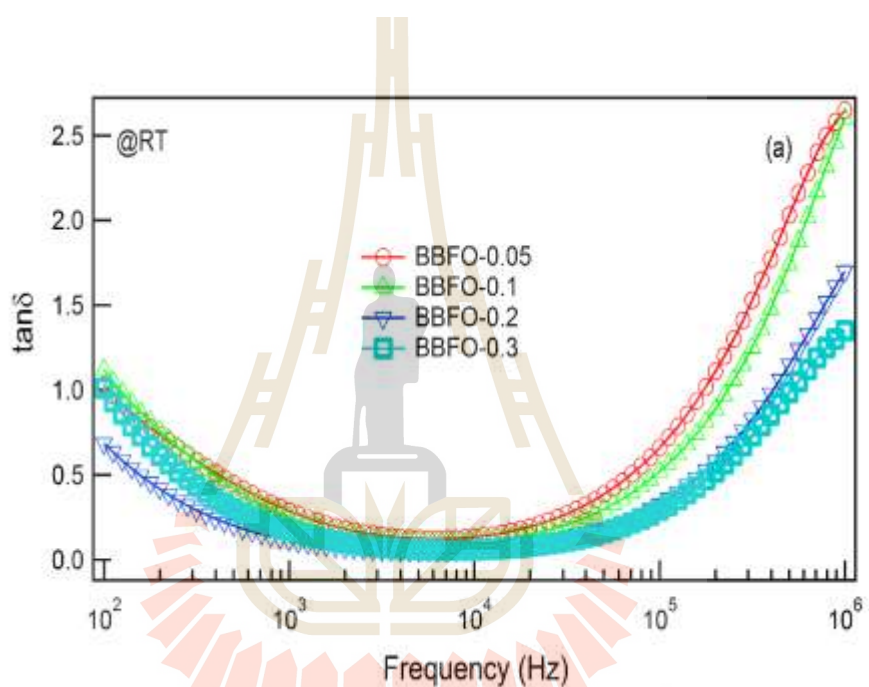
**Figure 2.6** (a) XANES spectra of  $\text{Bi}_{1-x}\text{La}_x\text{FeO}$  powders, (b) TEM image of BLFO 0.05 (Yotburut et al., 2014).

Figure 2.7 illustrates XRD pattern of both  $\text{BiFeO}_3$  powders.  $\text{BiFeO}_3$  ceramics after sintered showed the main phases of  $\text{BiFeO}_3$  which were observed in all conditions and revealed the rhombohedral structure with space group  $R3c$ . In pattern of BLFO-0.3 powder was observed the pure phase.



**Figure 2.7** XRD patterns of powders calcined at  $600^\circ\text{C}$  (a) for 3 hours and ceramics sintered at  $800^\circ\text{C}$  for 3 hours (b).

These samples exhibit high dielectric constant and their loss tangent is reasonably low especially in the frequency range between 2 – 20 kHz as shown in Figure 2.8; loss tangent of La doped BFO was measured by impedance analyzer (Yotburut et al., 2014). Both loss tangent graph will later be used to explain about changing of it under irradiations



**Figure 2.8** Trend of all BBFO-x (x = 0.05, 0.1, 0.2, 0.3) loss tangents with various frequency.

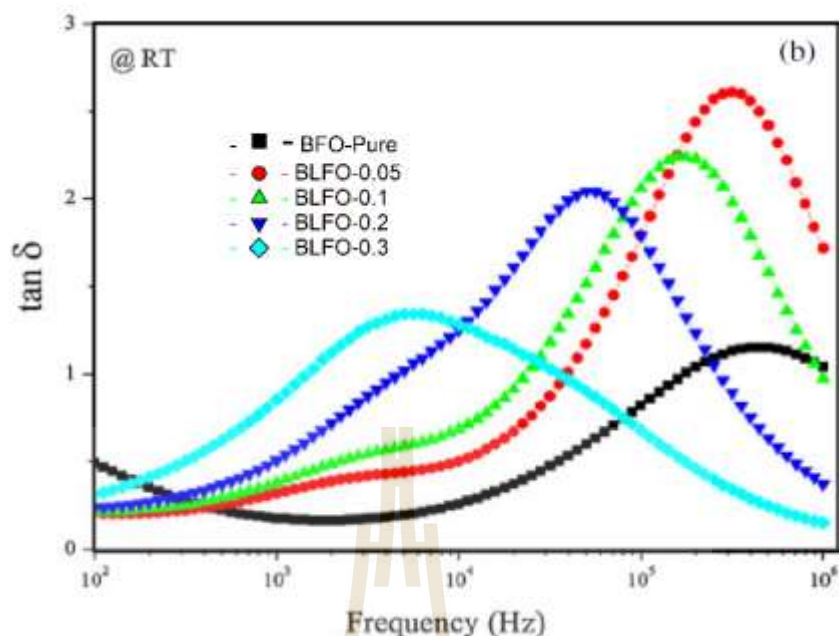


**Figure 2.9** Trend of all BLFO-x (x = 0, 0.05, 0.1, 0.2, 0.3) loss tangents with various frequency (Yotburut et al., 2014).

It was found that electrical measurement was very sensitive with the presence of grain boundaries in these materials (Lebeugle et al., 2007). Therefore, this performance was learned about dielectric constant when we activate by green, violet and ultraviolet light. Consequently, this research must be considered band gap which is between valence band and conduction band of  $\text{BiFeO}_3$ 's electronic structure. We found some researches which shown band gap. Direct band gap of  $\text{BiFeO}_3$  was reported to be around 2.81 eV at room temperature from the absorption of light at wavelength of 442 nm (Kumar et al., 2008). In 2009, Choi and their group also reported direct band gap of around 2.67 eV by using optical absorption measurement (Choi et al., 2009).  $\text{BiFeO}_3$ 's indirect band gap was calculated by using density-functional based screened exchange method to be approximate 2.8 eV (Clark et al., 2010).

For the thin-film aspects, a thin film is defined as a layer of materials ranging thickness fraction from a nanoscale (monolayer) to many micrometer. BiFeO<sub>3</sub> thin films were grown by many techniques on several substrates such as SrTiO<sub>3</sub> (STO), SrRuO<sub>3</sub> (SRO), and DyScO<sub>3</sub> (DSO). They find thickness of thin film by x-ray diffraction (XRD). In Ref. (Chu et al., 2007), films ranging from 2 to 600 nm were grown on (001) STO and (110) DSO substrates by using pulsed laser deposition at 700 degrees Celsius in oxygen partial pressure of around 100 mTorr. Local piezoelectric properties and surface morphology of BiFeO<sub>3</sub> were surveyed by using atomic force microscope (AFM). For study of band gap, BiFeO<sub>3</sub> thin film was deposited on SrRuO<sub>3</sub>-buffered (111) SrTiO<sub>3</sub> substrate. The BiFeO<sub>3</sub> was described by the Lorentz model received by fitting spectra data. The optical band gap of this BiFeO<sub>3</sub> thin film was reported to be around 2.68 eV. And then Ref, (Xu et al., 2014) that nearly with Zelezny and their groups were determined its band gab about 2.75 to 2.70 eV, varying temperature from 300 K to 775 K (Zelezny et al., 2010). At only 300 K, Basu and their research group identified its direct band gap in visible range for 2.667±0.005 eV (Basu et al., 2008). Then, they believed to be influenced by near-band gap transitions and depended on other substrate. The phase-pure BiFeO<sub>3</sub> thin film in thickness range of 50 – 500 nm on (100) STO substrates was grown by pulsed laser deposition (PLD). They need to ensure heteroepitaxial growth on substrate. Then, the SrRuO<sub>3</sub> (SRO) was chosen as a substrate for conducting perovskite oxide electrode. The effect of this constrained crystallographic state in this BiFeO<sub>3</sub> layer were investigated such as ferroelectric properties were characterized by using polarization hysteresis. Then, they can observed the remnant polarization which has order of magnitude higher than bulk BiFeO<sub>3</sub>. BiFeO<sub>3</sub> was highest reported value about of 6.1 μC/cm<sup>2</sup>. This ensures that they

measured the polarization characteristics under a pulsed probe condition, which is less similarly to be convoluted by leakage and nonlinear dielectric effects (Wang et al., 2003).

## **2.2 Capacitance enhancement under UV irradiation and negative electron compressibility**

This part will later be related to our study of the dielectric response of bismuth ferrite-based materials under green, violet light irradiations and varies intensities of both beams. In the same time, we vary frequencies of oscillation of alternating circuit (AC) but fix voltage between electrodes. Subsequently, bismuth ferrite materials were found to show a good response under green and violet light irradiation. The next step, we try to observe mechanism of changing in dielectric on electronic structure with light by using photoemission spectroscopy (PES).

From the previous work in our group (Masingboon et al., 2013), capacitance and loss tangent of  $\text{CaCu}_3\text{Ti}_4\text{O}_{12}$  (CCTO) were studied under violet irradiation at 1– 100 kHz because light-irradiation has been used to induce an enhancement of dielectric constant of  $\text{SrTiO}_3$  (Takesada et al., 2003; Hasegawa et al., 2003). And then, capacitance and loss tangent of CCTO were observed to be increased up to 22% and 19% respectively when measured at 1 kHz and under violet irradiation (violet laser) as shown in Figure 2.10. Intensity of this laser beam is about  $0.2 \text{ W/cm}^2$ . The beam profile of violet light laser was approximate circular with around 4 mm in diameter.

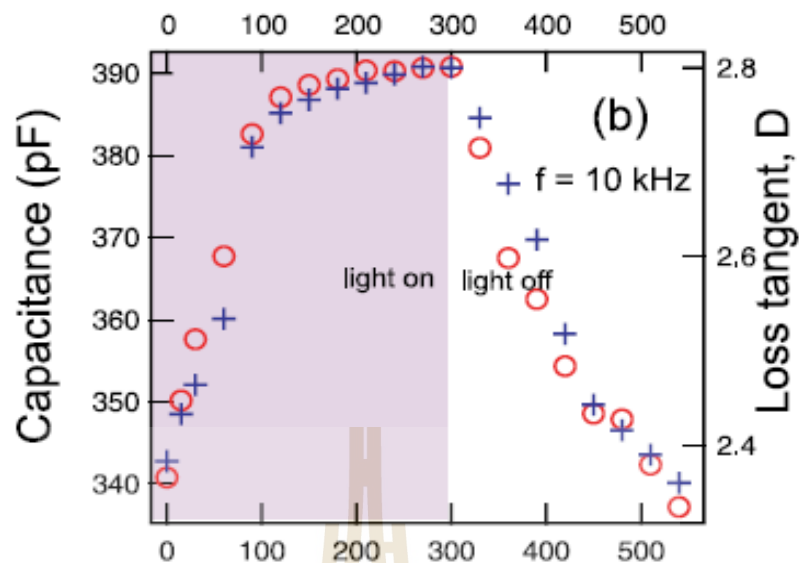


**Figure 2.10** Capacitance and loss tangent of CCTO at 1000 Hz (Masingboon et al., 2013).

From this graph, capacitance can be seen to get nearly saturated after 6 minutes of exposure. Upon irradiation, the dielectric responses quickly and after turning off the light, the trend of decreasing capacitance and loss tangent looks similar to an exponential decay graph. It was suggested that this could be used as a sensor.

Correspondingly (Figure 2.11), photoemission spectra of CCTO were measured with photon energy of 60 eV at Advanced Light Source (ALS). Upon increasing the dose of UV irradiation, the  $O_{2p}$  peak (region A) becomes lower but oxygen vacancy states (region B) becomes higher. This phenomena was associated with features found in both  $SrTiO_3$  (Aiura et al., 2002; Meevasana et al., 2010; Meevasana et al., 2011; Santander-Syro et al., 2010) and  $KTaO_3$  (King et al., 2012).

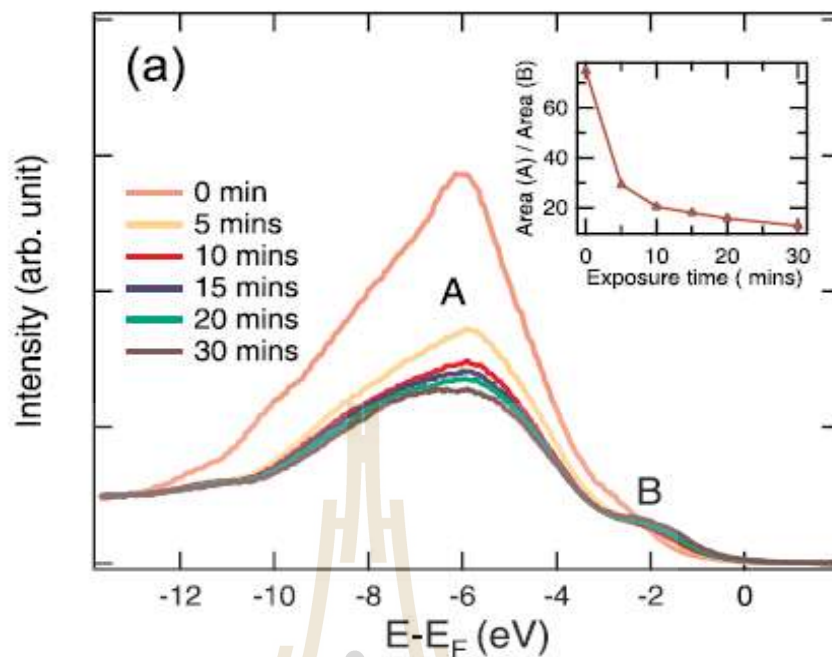


**Figure 2.11** Photoemission spectroscopy of CCTO at Advanced Light Source (ALS) (Masingboon et al., 2013).

Later the resistance of CCTO under irradiation was also measured to check whether it became more conductive under irradiation. To measure the resistance, the electrodes as shown in Figure 2.12 were made by using electron sputtering coater. Then, sample was exposed to the incident light (zeroth order) at  $2.02 \times 10^{-7}$  mbar at Synchrotron Light Research Institute (SLRI) for checking the resistance ( $R$ ) changes of the sample. Trend of resistance change under irradiation is shown in Figure 2.12.

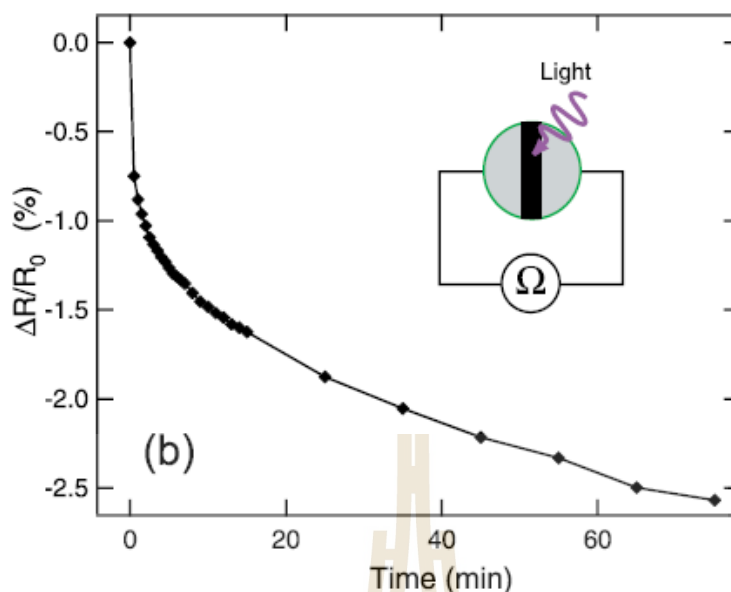


**Figure 2.12** The time dependence of resistance of CCTO upon exposure to light at SLRI (Masingboon et al., 2013).

That above study was originally motivated by two-dimensional conductivity found in  $\text{LaAlO}_3/\text{SrTiO}_3$  systems. Delta-doping studies and scanning conductance microscopy experiments show that it is conductive at the interface. This conductive layer or called two-dimensional electron gas (2DEG) occurs in a few nanometers (nm) (Basletic et al., 2008; Sing et al., 2009; Fix et al., 2009). In Ref (Li et al., 2010), they also proposed negative compressibility at interface between  $\text{LaAlO}_3$  and  $\text{SrTiO}_3$ . Then, this research defined the equation for calculating NEC which is caused by the exchange interaction. This emergent effect required to add an  $e^-$  to a sample plate. The reaction may be effected to charge capacitor with charging  $e^-$  does not simply require a change in voltage across the capacitor because of thermodynamic density of state (TDOS) in 2D system (only x-y axis, not thickness). Charging of capacitor required extra voltage  $\frac{d\mu}{e^{-A}}$ . This feature cause to increase of capacitance when interface of both

compound were biased by applying voltage. Then, they defined the minute capacitance as quantum capacitance ( $C_q$ ). As following simple capacitor in series circuit, this circuit have two capacitors which is series connecting. They offer this equation for explaining capacitance of measurement system when  $C_q$  appear in system.

$$\frac{1}{C_{\text{total}}} = \frac{1}{C_{\text{geom}}} + \frac{1}{C_q} \quad (2)$$

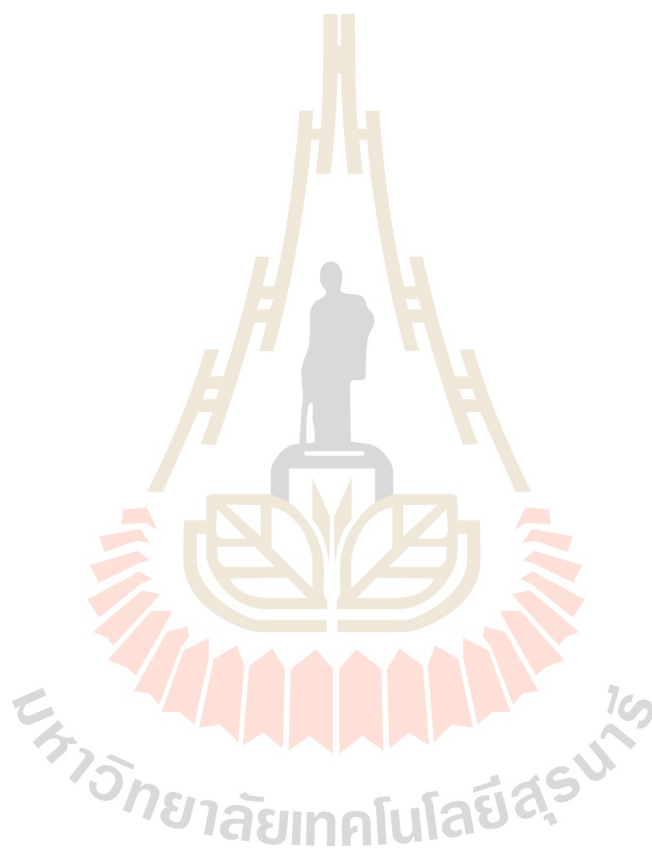
where  $C_{\text{total}}$  is enhanced capacitance when samples were exposed by light,  $C_{\text{geom}}$  is geometric capacitance and  $C_q = Ae^2 \frac{dn}{d\mu}$  (where  $A$  is effective area,  $e$  is electron charge,  $n$  is carrier density and  $\mu$  is chemical potential).

If  $\frac{dn}{d\mu}$  are positive, the quantum capacitance ( $C_q$ ) will diminish it's classical capacitance value (geometric capacitance:  $C_{\text{geom}}$ ). However, they observed enhancement capacitance ( $C_{\text{total}}$ ). That  $\frac{dn}{d\mu}$  should be negative compressibility more than positive compressibility.

Then, capacitance of a capacitor with this 2DEG inside was observed to increase up to 40 % from the capacitor without this 2DEG. In 2015, negative electron compressibility (NEC) was observed in  $\text{WSe}_2$  (Riley et al., 2015). This effect may help explaining the decreasing of resistance in CCTO. In the  $\text{WSe}_2$  measurement, when Fermi surface area (which can be used to calculate density state of electron) increases under doping alkaline metal, shifting of maximum valence band will approach Fermi level as shown in Figure 3.17. In conclusion of (Masingboon et al., 2013), they proposed quantum capacitance ( $C_q$ ) for explaining enhancement capacitance of CCTO. However, the proposed  $C_q$  has not been proved yet. This research in chapter IV, quantum capacitance will be calculated by using equation (2) was compared with the

result of electronic structure. Maximum valence band and chemical potential were shifted to Fermi level.

We anticipate that our samples will have these properties. If these samples have this property, this study of polycrystalline BFO will be different from the previous ones which focused only on surfaces/interfaces of single crystals.



# CHAPTER III

## METHODOLOGY AND MEASUREMENT

This chapter describes the materials and methods used in this research. We start with the preparation of  $\text{BiFeO}_3$  samples, then the capacitance measurement under irradiation, and electronic structure measurement by using photoemission spectroscopy (PES) at beamline 3.2 in Synchrotron Light Research Institute (SLRI).

### 3.1 Sample growth/ Samples preparation

In this work, the bismuth ferrite-based materials were grown by Miss. Benjaporn Yotburut in Prof. Dr. Santi Maensiri's group as described in the following.

Bismuth ferrite doped with lanthanum (La) or BLFO ( $\text{Bi}_{1-x}\text{La}_x\text{FeO}_3$  powder with  $x = 0.05, 0.1, 0.2, 0.3$ : abbreviated as BLFO-0.05, BLFO-0.1, BLFO-0.2, BLFO-0.3) were prepared by a simple co-precipitation method. Stoichiometric amounts of starting materials corresponding to each composition were blended in de-ionized water using magnetic stirrer to form a solution at room temperature. Then, nitric acid and PEG were added to the solution. After that, the resulting precursor was dried in an oven at 70 degrees Celsius. This powder was calcined in air at 600 degrees Celsius for 3 hours and was sintered at 800 degrees Celsius for 3 hours in air. Average grain size of bismuth ferrite doped lanthanum decreases with increasing quantity La (Yotburut et al., 2014). The average grain size of them is about 4-5  $\mu\text{m}$  in diameter. Finally, bismuth ferrite doped with barium (Ba) or BBFO ( $\text{Bi}_{1-x}\text{Ba}_x\text{FeO}_3$  powder with  $x = 0.05, 0.1, 0.2, 0.3$ :

abbreviated as BBFO-0.05, BBFO-0.1, BBFO-0.2, BBFO-0.3) were also prepared by a simple coprecipitation method. More detail can be read from (Yotburut et al., 2014). Band gap of the bismuth ferrite was reported to be indirect band gap of around 2.8 eV (Clark et al., 2010). Therefore, photon energy which is higher than 2.8 eV but lower than work function is suitable for observing any photoconductivity effect and oxygen vacancy.

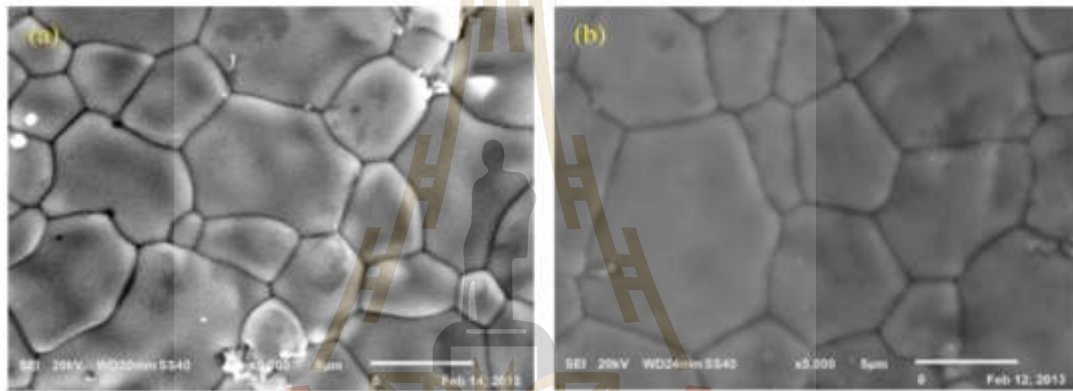


**Figure 3.1** (a) SEM picture of  $\text{BiFeO}_3$  and (b) SEM picture of BLFO-0.05 (Yotburut et al., 2014).

In the process before measurement, we tried to determine same thickness of all samples for about 0.8 mm in parallel for decreasing air gap between surface sample and surface of ITO electrode when measured. All these samples had the same thickness. Samples can be ignored about thickness effect in this measurement.



**Figure 3.2** Bismuth ferrite-based materials.

Process of preparation samples showed in below

- We polished these samples to determine the thickness and tried to make parallel samples by using highest resolute sand paper and this tool.



**Figure 3.3** Tool for determining thickness of samples.

- We polished these samples to smooth the surface and decrease air gap as much as we could do by using this equipment, silk cloth and diamond jell as shown in Figure 3.4. If we do not polish these surfaces, larger error will occur during capacitance measurement.



**Figure 3.4** Polishing equipment (a), diamond jell (b).

- We then cleaned samples by soaking them with acetone and ethyl alcohol and putting them in ultrasonic cleaner. After that, we dried samples by using hot plate at 70 °C. (This temperature must be less than phase transition temperature).

- Samples were coated with Au on one side of samples to be the bottom electrode by using electron sputtering.

### 3.2 Impedance analyzer measurement

Impedance analyzer was used for measuring dielectric constants (capacitance (C) and loss tangent (D)). We detected any change of these values as the following.

- Vary frequency of alternating current: 1,000 Hz, 10000 Hz, 100,000 Hz and 1000,000 Hz. We set voltage between 2 electrodes to be 1 Volt which should be suitable for these samples (Kemet Corporation, 2014).

- Vary photon energy of irradiations (green and violet irradiations) to observe changes in capacitance and loss tangent.

- Vary intensities of irradiation to observe changes in capacitance and loss tangent.

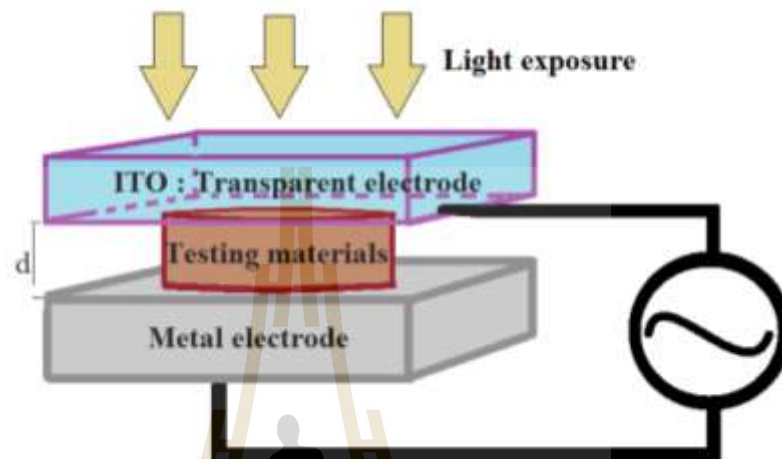


**Figure 3.5** Schematic diagram of capacitance and loss tangent measurements.

### 3.2.1 Impedance analyzer

This machine can be set to different measurement modes such as impedance ( $Z$ ), resistance ( $R$ ), conductance ( $G$ ), inductance ( $L$ ), series capacitance ( $C_s$ ) etc. In this research, we measure dielectric constants in the mode of parallel capacitance ( $C_p$ ) and loss tangent ( $D$ ). This machine can measure the range of frequency between 40 Hz- 110 MHz, and voltage between 5 mV- 1 V. Impedance analyzer was manufactured by Agilent Technology in Japan in 2003 (Agilent Technologies, 2003).

### 3.2.2 Fixture

Fixture is a device used for holding a sample and can be connected with impedance analyzer. Fixture was designed for keeping the sample to be in between two electrodes. Top-side electrode is either transparent indium-tin-oxide (ITO) or F-doped tin oxide. This side would be exposed to irradiation. Another side is metal electrode;

this surface of metal electrode must be smooth to minimize any air gap which can occur at the interface between surface sample and surface of this electrode as shown in Figure 3.6.

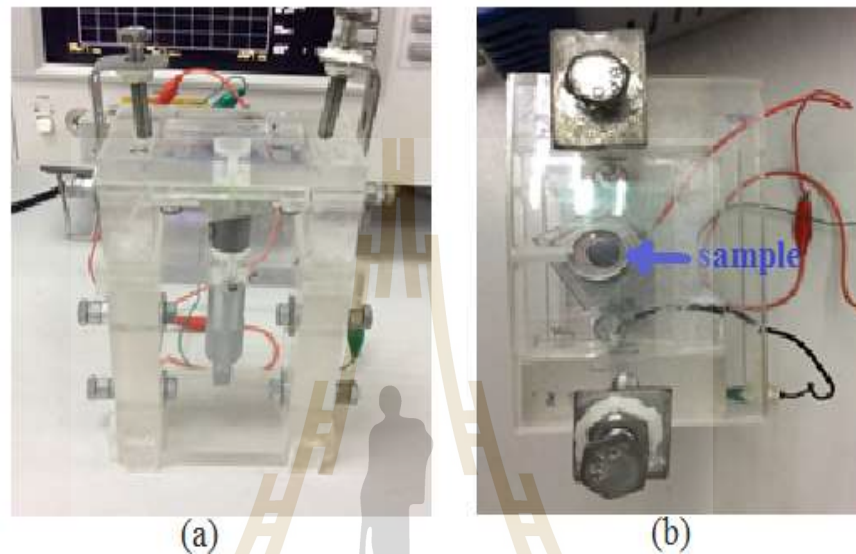


**Figure 3.6** Front view (a) and top view (b) of fixture.

### 3.2.3 Capacitance

Capacitance (C) is important value for this thesis because we measure and observe the changing capacitance of Bismuth ferrite materials. C is the ability of the device to store an electrical charge. Any object which can be electrically charged exhibits capacitance. A common form of energy storage device is a parallel-plate capacitor. Therefore, the capacitance (C) is given by

$$C = \frac{\epsilon_r \epsilon_0 A}{d} \quad (3)$$

where C is capacitance (F or farad),  $\epsilon_r$  is dielectric permittivity of sample materials (F/m),  $\epsilon_0$  is permittivity of vacuum ( $8.854 \times 10^{-12}$  F/m), A is area surface ( $m^2$ ) and d is distance between to electrode (m).

Generally, capacitance is identified into 2 modes which are series capacitance and parallel capacitance. In this research, we used parallel circuit mode for measuring bismuth-ferrite based materials. We have considered this circuit as follows: Firstly, we consider real diagram of bismuth ferrite-based materials. We get this diagram as shown in Figure 3.7.

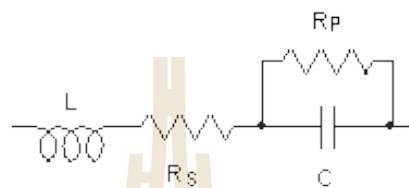


**Figure 3.7** Diagram of bismuth ferrite-based materials same as capacitor.

Secondly, we can ignore inductive part (L) of this circuit because the frequencies in our measurement are lower than self-resonance frequency of bismuth ferrite-based materials (about 30 MHz). So, Inductive part cannot be observed in measurement because of the above reason. This circuit can be simplified in to this diagram as shown in Figure 3.8.

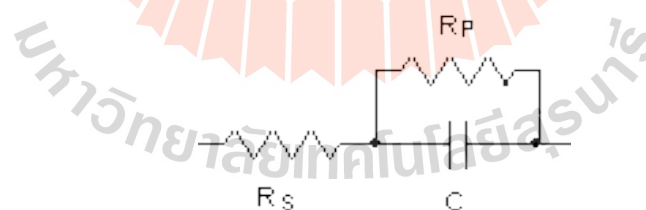


**Figure 3.8** Diagram in bismuth ferrite-based materials when we ignore inductive part.

Finally, we can consider the impedance of bismuth ferrite based materials into more simple form. In the case of samples have high impedance, the parallel resistance ( $R_p$ ) will be dominated compare to series resistance ( $R_s$ ). So, we can ignore  $R_s$  part in our setup. Therefore, the circuit will be remained only parallel capacitance ( $C_p$ ).

On the other hand, if sample have low impedance,  $R_s$  will be dominated more than  $R_p$ . We can ignore  $R_p$  part. Therefore, the circuit will be remained series capacitance ( $C_s$ ). In conclusion, the capacitance of bismuth ferrite materials samples can be obtained using parallel capacitance mode ( $C_p$ ).

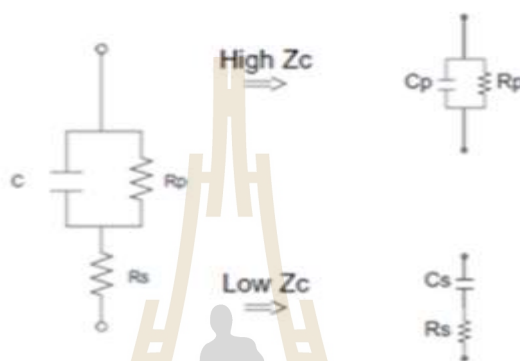


**Figure 3.9** Diagram in bismuth ferrite-based materials when we consider impedance. (Picture from <http://cp.literature.agilent.com/litweb/pdf/5950-3000.pdf>).

### 3.2.4 Quality factor

The equation defines Q as the following.

$Q = \omega$  energy stored/average power dissipated

$$Q = \omega \frac{\text{energy stored}}{\text{average power dissipated}} \quad (4)$$

For parallel circuit,

$$\text{Energy stored is } E = \frac{1}{2} CV^2 \quad (5)$$

$$\text{And, average power dissipated is } P_{\text{avg}} = \frac{1}{2} I^2 R = \frac{V^2}{2R} \quad (6)$$

Therefore, when equations (4) and (5) substitute in equation (6). And then, we will get

$$Q = \omega \frac{E}{P_{\text{avg}}}$$

$$= \omega \frac{\frac{1}{2}CV^2}{\frac{V^2}{2R}} = \omega C_p R_p \quad (7)$$

So, we get quality factor (Q) =  $\omega C_p R_p$

Quality factor of some bismuth ferrite-based materials (real measurement)

In previous work, we measure resistance of bismuth-ferrite-based materials. Then this value is about 1 M $\Omega$ . Parallel capacitance mode ( $C_p$ ) and series capacitance mode ( $C_s$ ) are chosen for comparing of quality factor (Table 1).

**Table 1** Frequency, angular frequency, capacitance and quality factor from parallel capacitance mode ( $C_p$ ) and series capacitance mode ( $C_s$ ) in our measurement.

f (Hz)	$\omega$ (Hz)	C (pF)	Q from $C_p$	Q from $C_s$
1 kHz	6280	400	2.512	0.3980
10 kHz	62800	320	20.1	0.0497
100 kHz	628000	200	125.6	0.0079
1 MHz	6280000	120	628	0.0016

This result ensures that parallel capacitance mode ( $C_p$ ) is suitable for bismuth-ferrite-based materials samples.

### 3.2.5 Loss tangent

Loss tangent or dissipation factor (D) is measurement of loss-rate of energy of oscillation mode. It has no unit. Reciprocal of loss tangent is quality factor. Therefore,

we can use these two parameters to refer suitable function in our measurement. Therefore, this equation is given by

$$D = \frac{1}{Q} \quad (8)$$

Quality factor (Q) is the parameter which can indicate quality of measurement. We can calculate Q by using this equation 9 which is used for parallel capacitance measurement mode.

$$Q = \omega C_p R_p \quad (9)$$

where  $\omega$  is angular frequency (Hz),  $C_p$  is parallel capacitance (F) and  $R_p$  is parallel resistance ( $\Omega$ ).

### 3.3 Photoemission spectroscopy

At beamline 3.2 (PES) of Synchrotron Light Research Institute (SLRI), there is a photoemission spectroscopy technique used for investigating  $O_{2p}$  states and oxygen vacancy states of maximum valence band in electronic structure. For this measurement, photon energy of ultraviolet irradiation was set at 60 eV. And the reference peak was  $C_{1s}$  peak for determinate position of all peak in electronic structure. For this measurement, photon energy of ultraviolet irradiation was set at 500 eV

After that, we exposed zeroth order light for activation surface samples then measured maximum valence band in electronic structure again. And then, we also observed the reference peak ( $C_{1s}$  peak) for ensure each peak's position. We use only 3 conditions of all samples for measurements which are  $BiFeO_3$  BBFO-0.05 and BLFO-0.05.

Operation at Synchrotron Light Research Institute (SLRI), Thailand has many steps.

After we finish dielectric measurement, the measurement processes are as the following.

- Clean these samples by using acetone, ethyl alcohol and ultrasonic cleaner.
- Prepare the samples by mounting it with the sample holder using TorrSeal epoxy and silver epoxy.
- Load the prepared samples to the ultrahigh vacuum (UHV) chamber and then pump the chamber until a pressure reaches around  $10^{-7}$  torr.
- Use the PES program control some parameter and collect the data after that we analyze data by IGOR program.

We had chance to measure electronic structure of thin-film's  $\text{BiFeO}_3$  and  $\text{BLFO-0.05}$  at Advanced Light Source (ALS), USA. The measurement processes are similar to above processes (where the pressure was around  $10^{-11}$  torr and temperature was around 100 K).

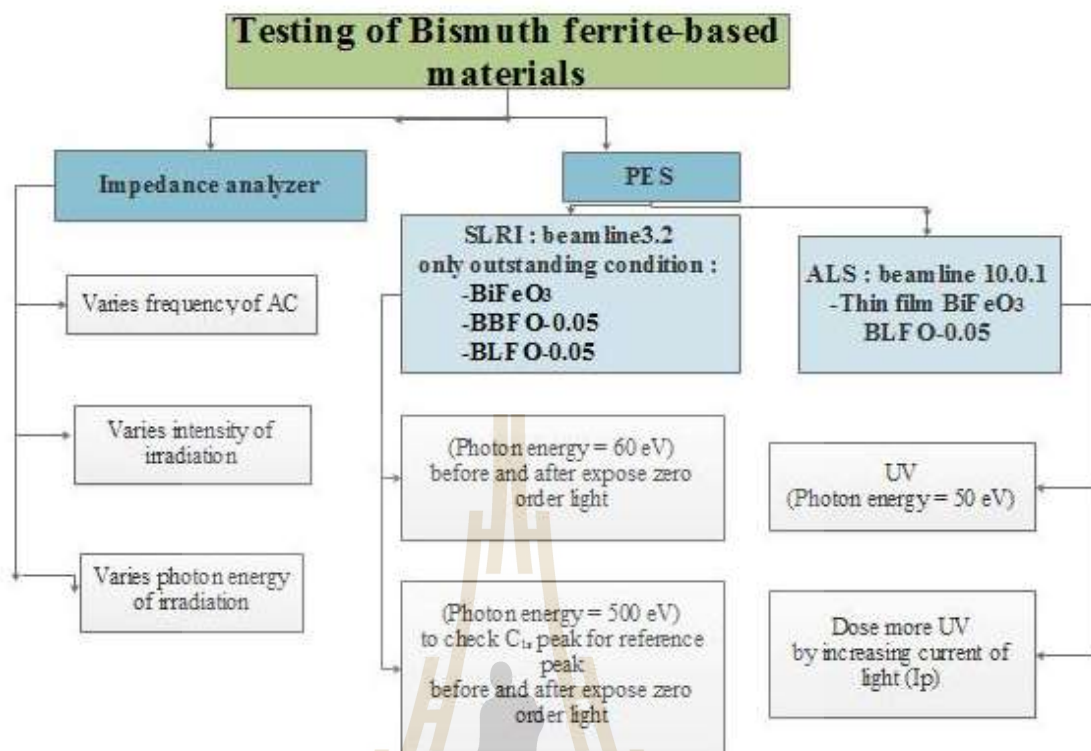


**Figure 3.10** Flow chart of conditions of measurement in this research.

This PES technique has many components, terms and capabilities to be introduced below; these will be used in the next chapter.

### 3.3.1 Photon energy

We measured maximum valence band and  $O_{2p}$  states of  $BiFeO_3$ ,  $BBFO-0.05$ , and  $BLFO-0.05$  by exposing UV light at 60 eV (SLRI) and 50 eV (ALS). We observed reference peak:  $C_{1s}$  (binding energy about 284.2 eV) of these samples by using photon energy of 500 eV (only at SLRI); this reference peak is useful for calibrating the binding energy of each sample in the case that charging effect occurs.

### 3.3.2 Zeroth order light

Zeroth order light is the mode that all frequencies of light from the undulator at a given gap size are used for the experiment (i.e. high intensity). We use this zeroth

order light when we want the change due to irradiation-induced effect to be large. For example, we observed position of valence band and  $C_{1s}$  both before and after applying zeroth order light to the BLFO sample.

### 3.3.3 Photoelectric effect

Photoelectric effect is the phenomenon that many materials emit electron when the sample surface is exposed with light. Then, electrons ejected from the occupied electron level on the surface of sample as shown in Figure 3.11. This process is called “photoelectric effect” or “photoemission effect”. The electrons ejected are called photoelectrons which have the kinetic energy, momentum and spin.

In this work, photoelectric effect is the result of light impact which is used in PES. Follow the principle, each electron have each finger print of itself. And then, we use to make sure about elements in each sample. Other than, we use for observing oxygen vacancy.

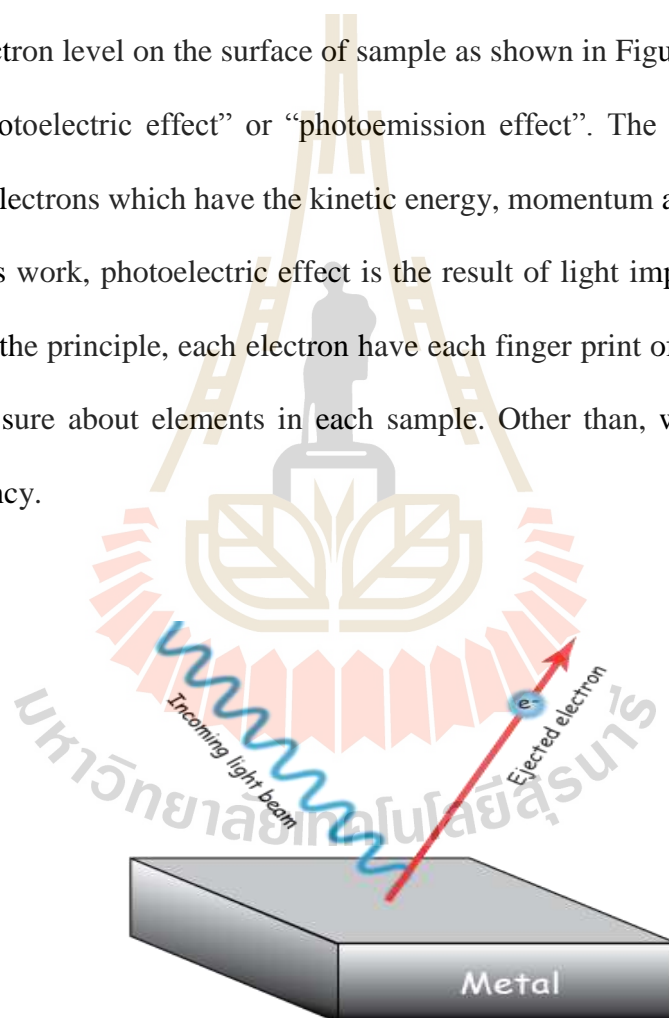


**Figure 3.11** Mechanism of photoelectric effect (picture from <https://www.emaze.com/@ALITQOQT/Photoelectric-Effect>).

### 3.3.4 Principles of photoemission spectroscopy

Photoemission spectroscopy (PES) may be known as photoelectron spectroscopy, referring to energy measurement of electrons which was emitted from sample test such as metal oxide materials etc. The photoelectric spectroscopy can check the change in valence band and some binding energies at specific elements. All photoelectron spectroscopy revolves around the general theme of surface analysis by measuring the ejected electrons. We can use this equation for explanation:

$$E_k = eV_s = h\nu - W - E_B \quad (10)$$

where  $W$  is work function (eV),  $h$  is Plank's constant,  $V_s$  is stopping potential,  $E_B$  is binding energy,  $E_k$  is kinetic energy of photo-electron,  $e$  is the electron charge and  $\nu$  is the frequency of incident light.

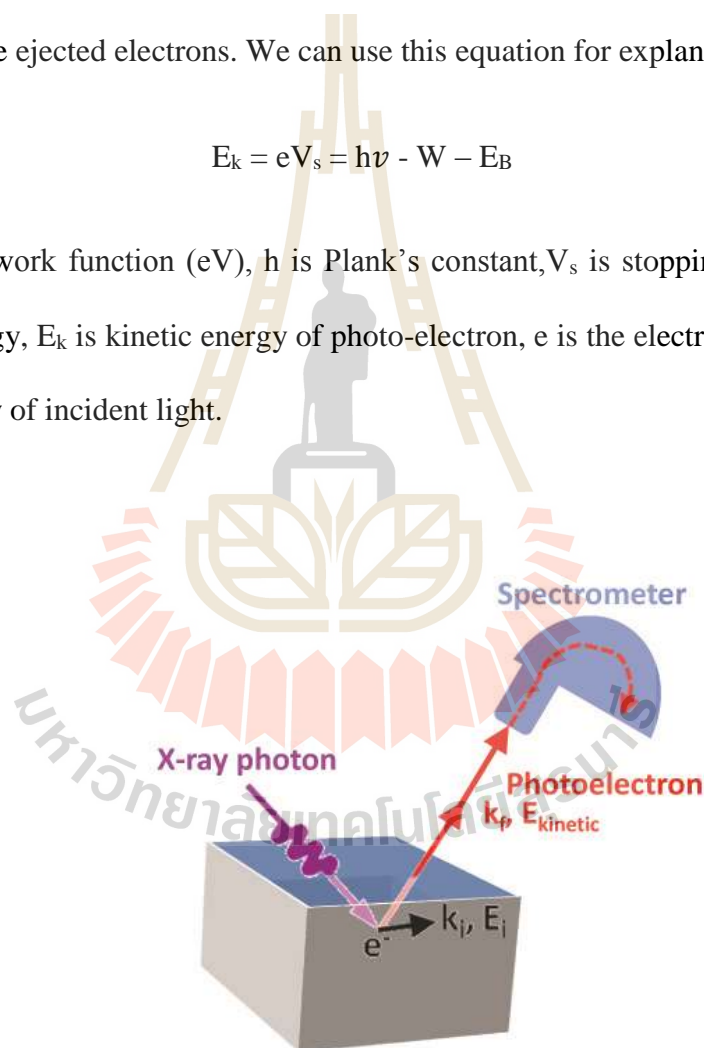


**Figure 3.12** Mechanism of photoemission spectroscopy (picture from <http://newscenter.lbl.gov/2011/08/24/harpes>).

### 3.3.5 Oxygen vacancy

Oxygen vacancy is important in the phenomena related to electrical conductivity and the general qualification in some metal oxides (Tanaka et al., 2002) when light exposed on surface of metal oxide. This light can activate oxygen out of surface. The oxidation state of oxygen is  $2^-$ . When these oxygen atoms escape from the surface of the materials, the surface will effectively be doped by electron. If these electrons can move around, the surface will become more conductive and increase capacitance. These oxygen vacancy states can be detected by photoemission spectroscopy (see Figure 2.11).

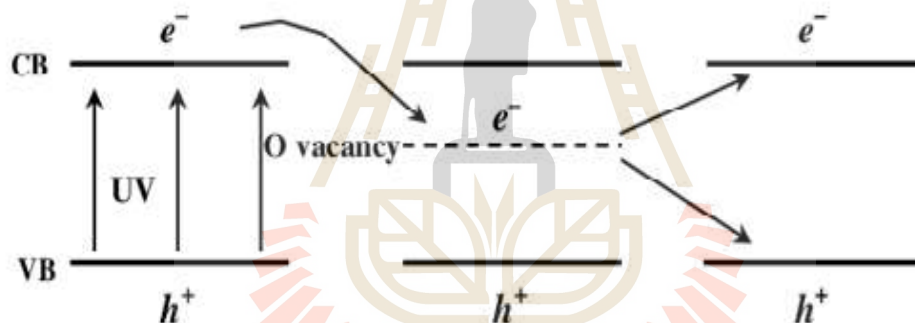


**Figure 3.13** The simplified models for the possible mechanisms of oxygen-vacancy formation (Tanaka et al., 2002).

### 3.3.6 Method to check the effect of negative electron compressibility

In this research, we will later propose negative electron compressibility as an origin which causes the enhancement in capacitance of bismuth ferrite-based materials. Negative electron compressibility may explain importance of exchange and correlation contributions to the total energy. However, thermodynamics of interacting electron system has been long theoretically appreciated. In low density regime only the exchange energy is enough to create a negative electron compressibility (NEC) for the

electron gas where exchange interactions dominate the kinetic energy (Eisenstein et al., 1991). In measurement, they biased and controlled voltage applied to the electrode between interface of  $\text{LaAlO}_3$  and  $\text{SrTiO}_3$  samples. Then, interface caused higher capacitance in system that came from the negative capacitance or quantum capacitance

( $C_q$ ):  $\frac{d\mu/dn}{e^{-A}}$  (Li et al., 2011). To understand this effect, we would like to give an analogy.

In the case of water which exhibits a *positive* mechanical compressibility, when pouring water into a glass, the level of water will be higher and higher due to the property of positive compressibility. However if it were the case of negative compressibility, the water level would be lower and lower upon pouring water and the glass would be able to store the water as long as the compressibility remained negative. In this case, it is the negative electron compressibility; one may replace the water in the above analogy by electron.

One method to check this effect is described in Li et al. (2011) where the capacitance of a capacitor with  $\text{LaAlO}_3/\text{SrTiO}_3$  interface was measured. This device has a top gate made of YBCO. Capacitance (C) versus top gate voltage ( $V_g$ ) measurement were performed at temperature 4.2 K. The tool can control density state of electron by using controllable bias voltage ( $V_g$ ) to creating two dimension electron system (setup sketch of the capacitance bridge as shown in Figure 3.14). Chemical potential shift would be calculated using equation 2 in Chapter II. In measurement, capacitance of this system will be increased with two-dimensional electron system. The 2 capacitors were connected in series. The capacitance will be increased when a bias voltage is applied. That capacitance increases because of quantum capacitance ( $C_q$ ). This term of  $C_q$  can be negative rather than positive.

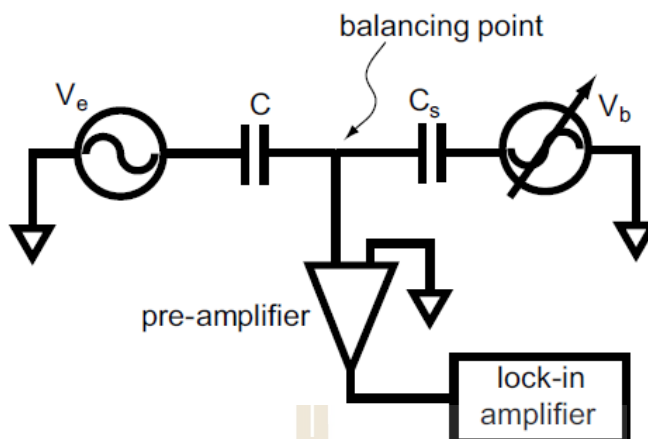


**Figure 3.14** Diagram of capacitance measurement (Li et al., 2011).

The NEC can also be measured by angle-resolved photoemission spectroscopy (ARPES). This technique is useful equipment for probing electronic structure and directly measure density states of electron in reciprocal space of solid materials. In Riley et al., 2015,  $\text{WSe}_2$  clearly showed the effect of negative electron compressibility when being doped by alkaline metal at the sample surface as shown in Figure 3.17(b). These maximum valance bands of  $\text{WSe}_2$  at K point will be shifted closer to  $E_F$  with increased doping alkaline metal on surface samples (instead of shifting away from  $E_F$  in other usual cases). Distinct shifting of valance bands,  $\Delta$ , was showed in Figure 3.17(c). The dispersion of two-dimensional electron gas was measured at momentum position along  $\Gamma$  point to K point direction. This showed density state of electron of 2DEG increase with increasing doping alkaline metal on surface as shown in Figure 3.17(a). Density state of electron ( $n$ ) can be calculated from the area of Fermi surface.

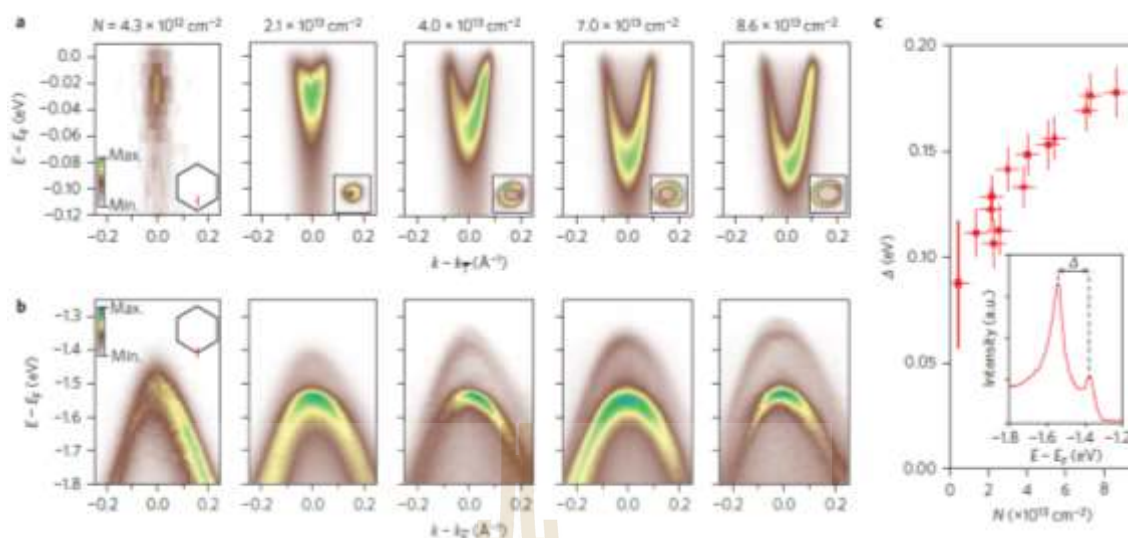


**Figure 3.15** Electronic structure of (a) Fermi surface, (b) valence band versus doping (Riley et al., 2015).

In this research, photoemission spectroscopy can also be used for observing  $C_{1s}$  peak and maximum valence band. We have limitation about samples and measurement. 2DEG of these samples may not be observed because samples are polycrystal (instead of single-crystal form); hence, the carrier density cannot be calculated from the Fermi surface (which can be obtained only from single-crystal samples). Therefore, electron density of state in our research cannot directly be calculated. However, in our case, oxygen vacancy states were created under UV irradiation, indicating that the electron density of state is larger, i.e. 2 electrons will be doped on surface because of oxidation number of oxygen is -2.

## **CHAPTER IV**

### **RESULTS AND DISCUSSION**

In this chapter, dielectric response measured by impedance analyzer will be explained and discussed. Then, percentage change of capacitance and loss tangent in each condition is plotted by Igor program. After that, oxygen vacancy states and negative electron compressibility (NEC) were investigated by using photoemission spectroscopy (PES) at beamline 3.2 in Synchrotron Light Research Institute (SLRI) and Advance Light Source (ALS).

#### **4.1 Dielectric measurement of bismuth ferrite-based materials by impedance analyzer**

Capacitance and loss tangent of these samples were measured with different conditions of 1) AC frequency of electrical source, 2) photon energy of irradiation and 3) intensity of irradiations. Changes in capacitance (C) and loss tangent (D) under laser irradiation will be described as the following.

##### **4.1.1 Bismuth ferrite (BiFeO<sub>3</sub>)**

Bismuth ferrite was measured to observe changes in C, D when the samples were exposed by each irradiation for 4 minutes and turned off light after that. Capacitance increased with increasing irradiation time. However, the trend of change in D is more complex; for example, loss tangent decreased under green irradiation but increased with violet light exposure at 10 kHz (see pages 39). Percentage changes of C

and D under green irradiation and violet irradiation were shown in Figure 4.2 (blue circles show capacitance and red plus show loss tangent).

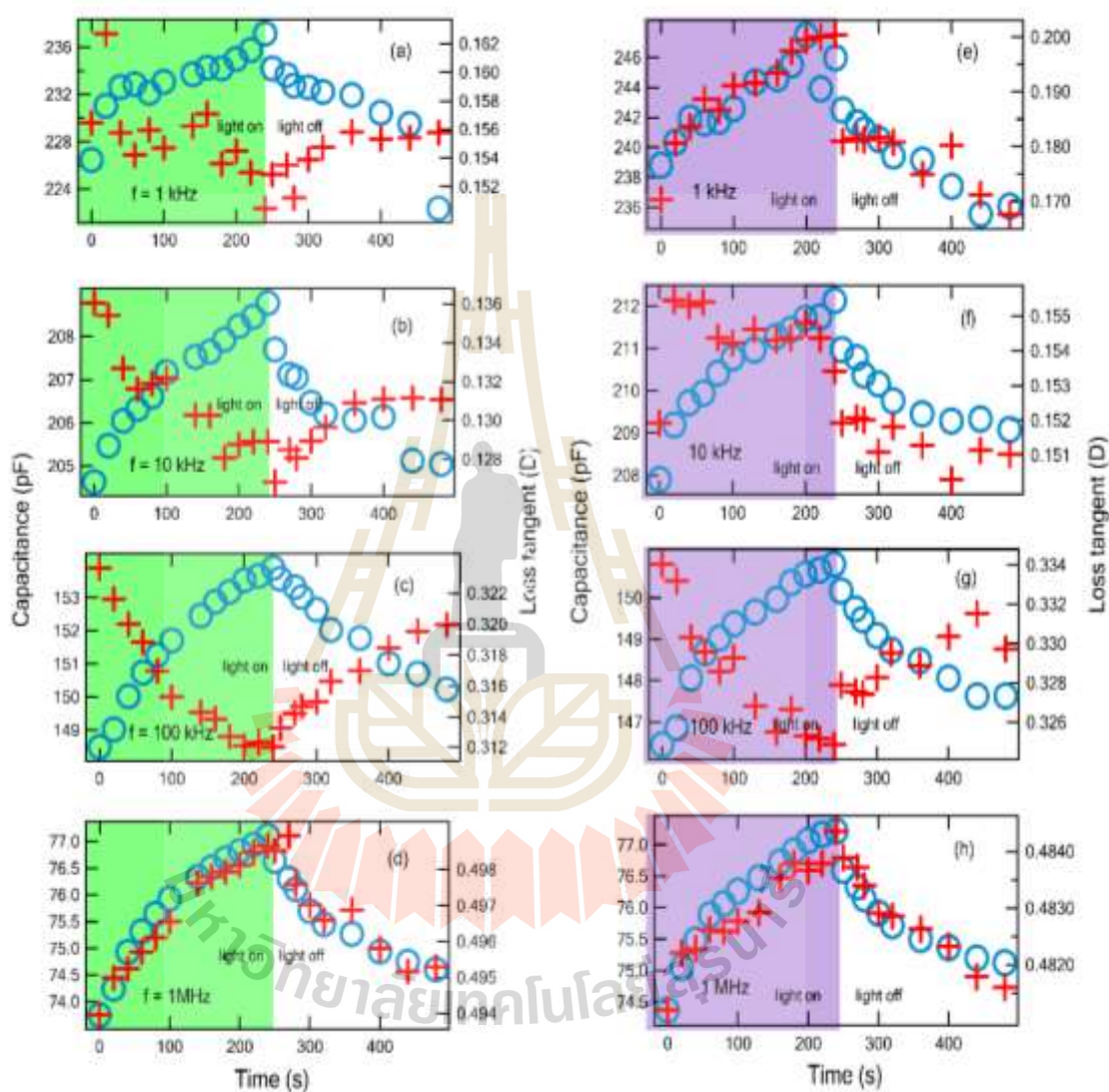


**Figure 4.1** Capacitance and loss tangent of BiFeO<sub>3</sub> under green irradiation approximate

$4.1 \frac{W}{\text{cm}^2}$  (a-d), under violet irradiation approximate  $1.8 \frac{W}{\text{cm}^2}$  (e-h).

Percentage changes of C and D of all measurement conditions were illustrated in Figure 4.2. Trends of capacitance and loss tangent under green irradiation are similar to

ones with under violet irradiation at 10, 100 and 1000 kHz. It appears that there is more current leakage under violet light irradiation than under green irradiation.

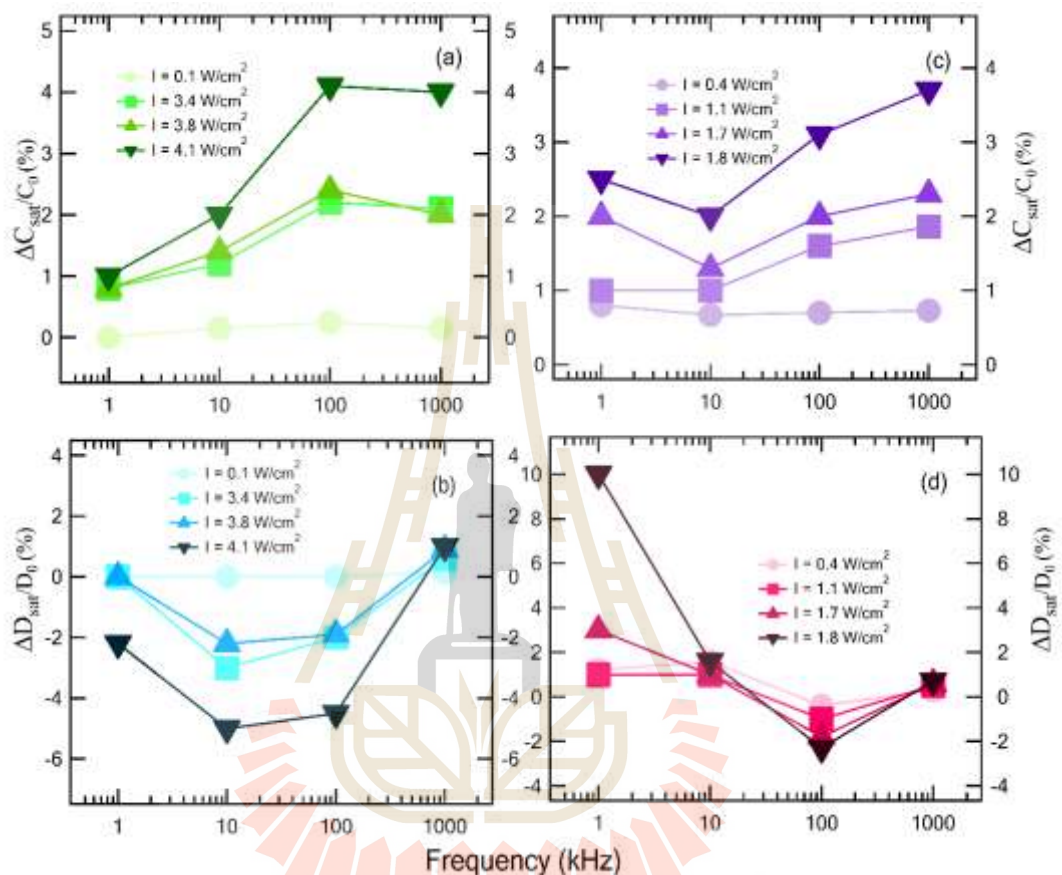


**Figure 4.2** Percentage change of capacitance and loss tangent of all conditions for BiFeO<sub>3</sub>.

#### 4.1.2 BBFO-0.05 (Bi<sub>0.95</sub>Ba<sub>0.05</sub>FeO<sub>3</sub>)

Capacitance and loss tangent of BBFO-0.05 were showed in Figure 4.3. It was found that, trends of changing under green and violet irradiations were similar at all frequencies. This change responds better under violet irradiation than green light. At 100 kHz, loss tangent (D) of both experiments decreased when increasing irradiation time.

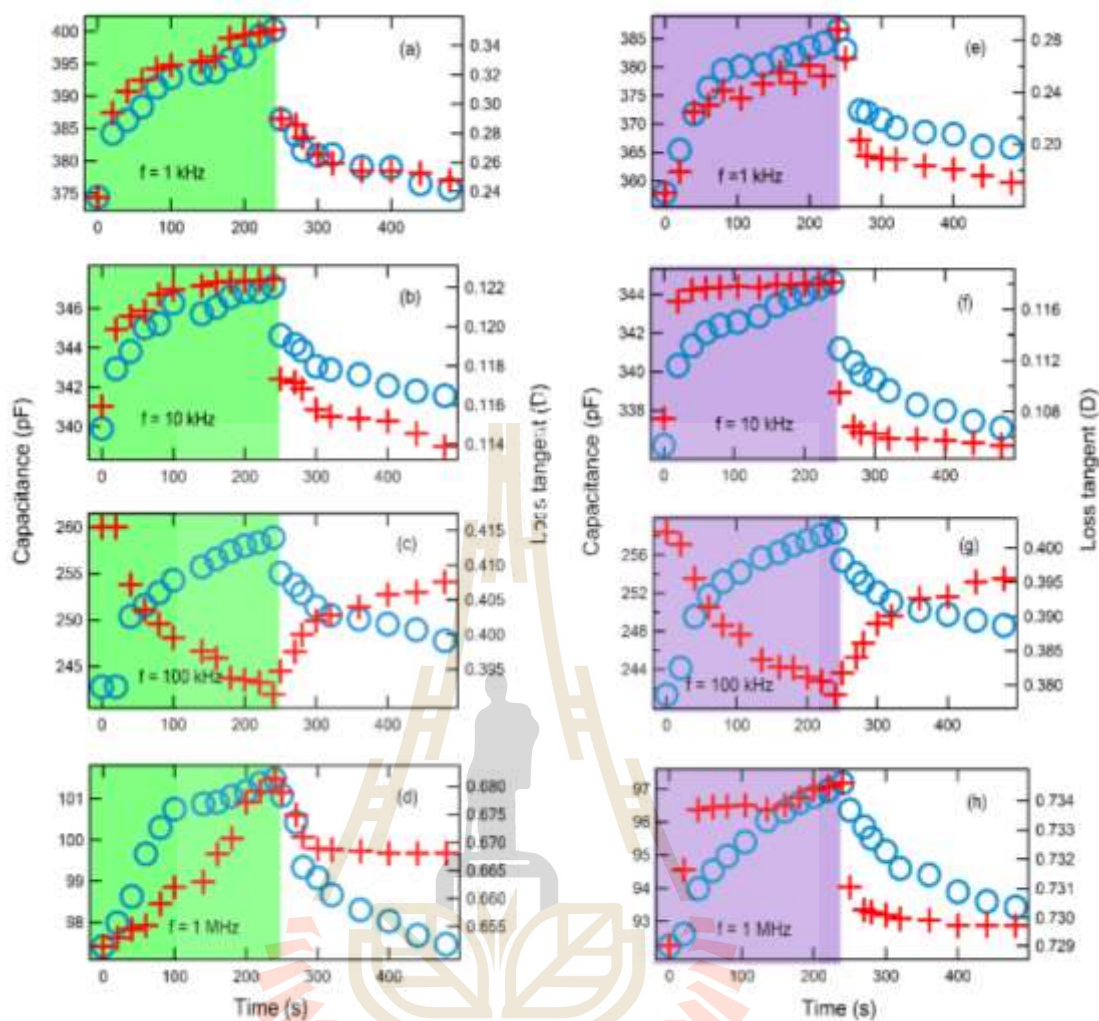


**Figure 4.3** Capacitance and loss tangent of BBFO-0.05 under green irradiation approximate  $4.1 \frac{\text{W}}{\text{cm}^2}$  (a-d), under violet irradiation approximate  $1.8 \frac{\text{W}}{\text{cm}^2}$  (e-h).

Percentage change of C and D of all measurement conditions were reported in Figure 4.4. It was found that, trends of changing in all intensities of light are same pattern at all frequencies. This change responds better under violet irradiation than green light. Capacitance and loss tangent can increase at least 8% and more than 60% at 1 kHz respectively under violet irradiation. Loss tangent of this condition is the highest among all the samples measured in this thesis.

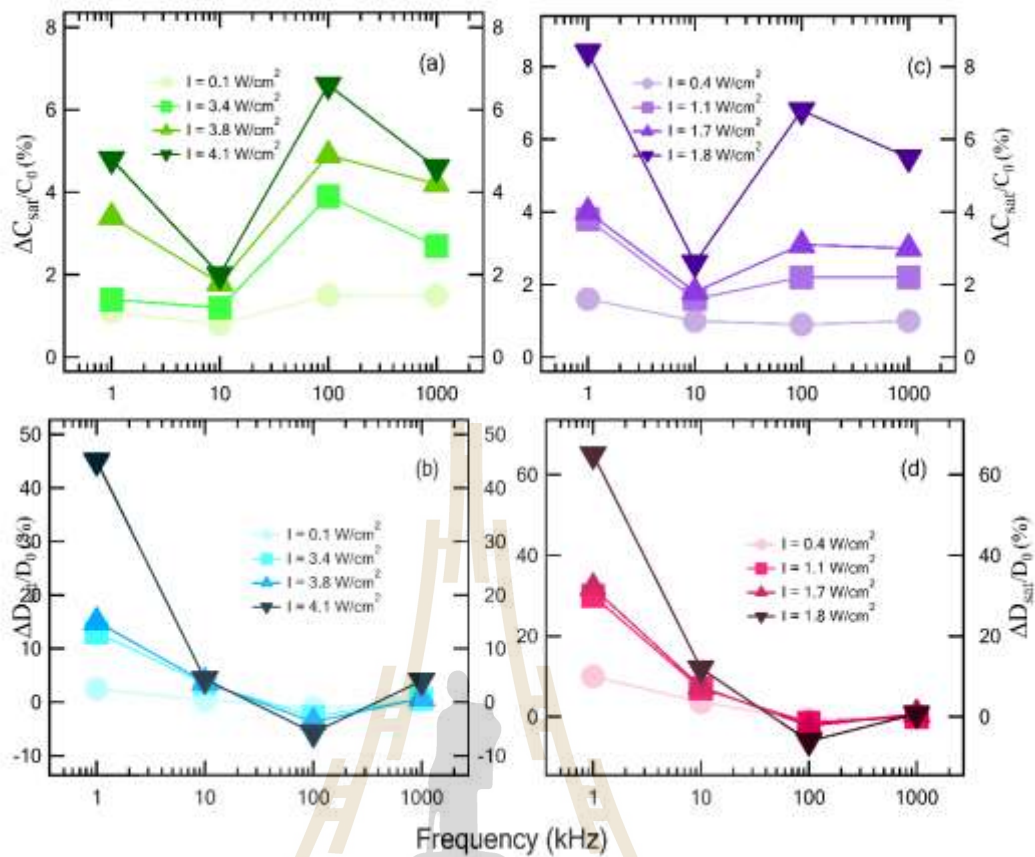


**Figure 4.4** Percentage change of capacitance and loss tangent under different conditions for BBFO-0.05.

### 4.1.3 BBFO-0.1 ( $\text{Bi}_{0.9}\text{Ba}_{0.1}\text{FeO}_3$ )

Trends of changing of BBFO-0.1 under green and violet light are quite similar changing as shown in Figure 4.5. C and D can respond to green better than violet irradiation.

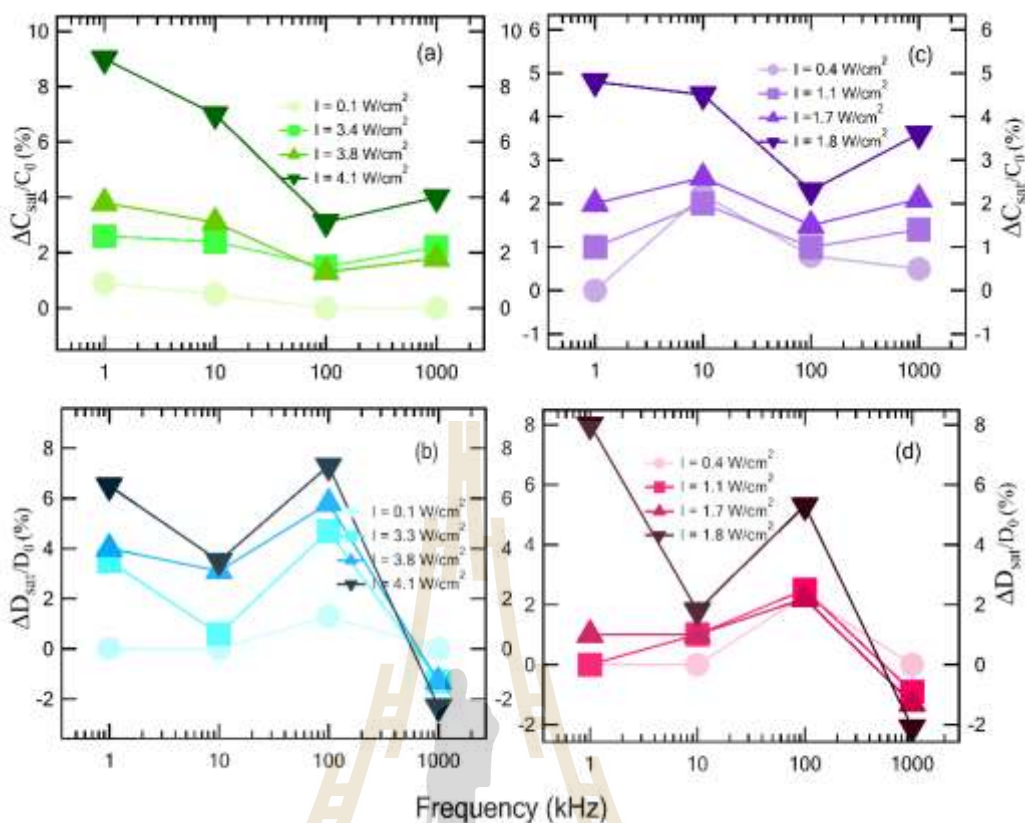


**Figure 4.5** Percentage change of capacitance and loss tangent under all conditions for BBFO-0.1.

#### 4.1.4 BBFO-0.2 ( $\text{Bi}_{0.8}\text{Ba}_{0.2}\text{FeO}_3$ )

In Figure 4.6, percentage change of capacitance increases upon increasing measurement frequency. In contrast, percentage change of loss tangent decreases upon increasing measurement frequency. C can increase to 5% at 1 MHz and D can increase to 30% at 1 kHz under violet irradiation.

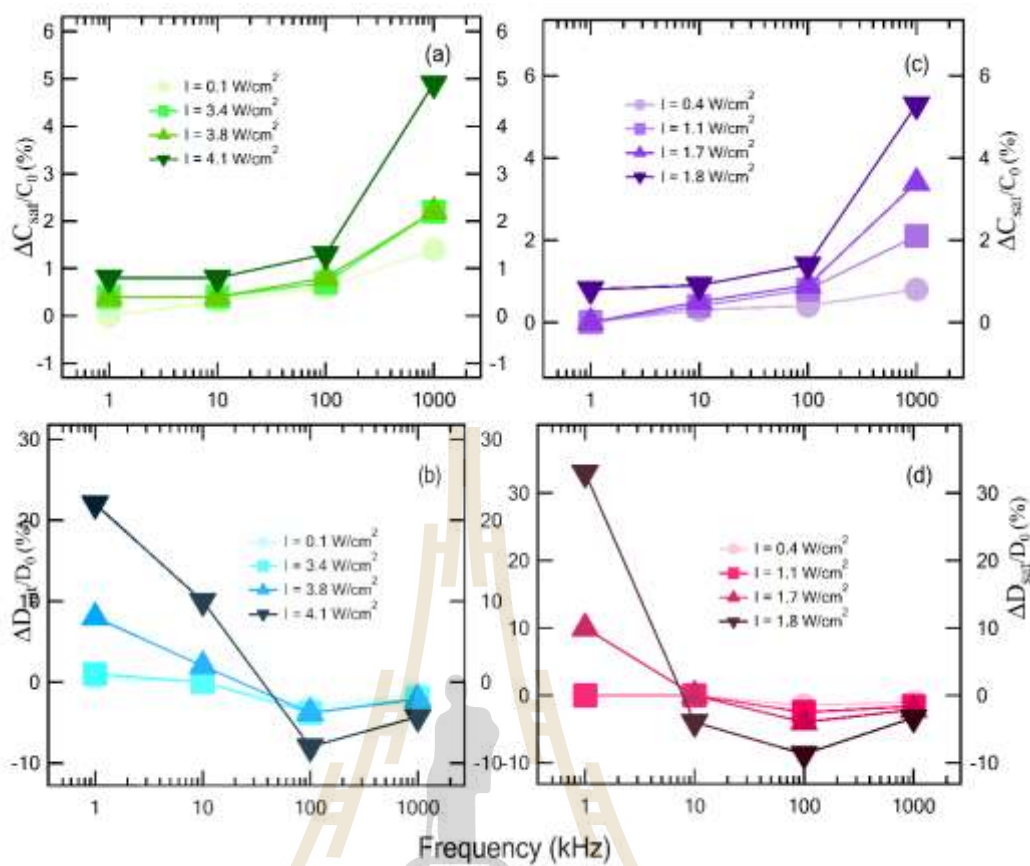


**Figure 4.6** Percentage change of capacitance and loss tangent under different conditions for BBFO-0.2.

#### 4.1.5 BBFO-0.3 ( $\text{Bi}_{0.7}\text{Ba}_{0.3}\text{FeO}_3$ )

Capacitance of this condition increases with increasing measurement frequency. Then, it can increase at least up to 6% under green irradiation.

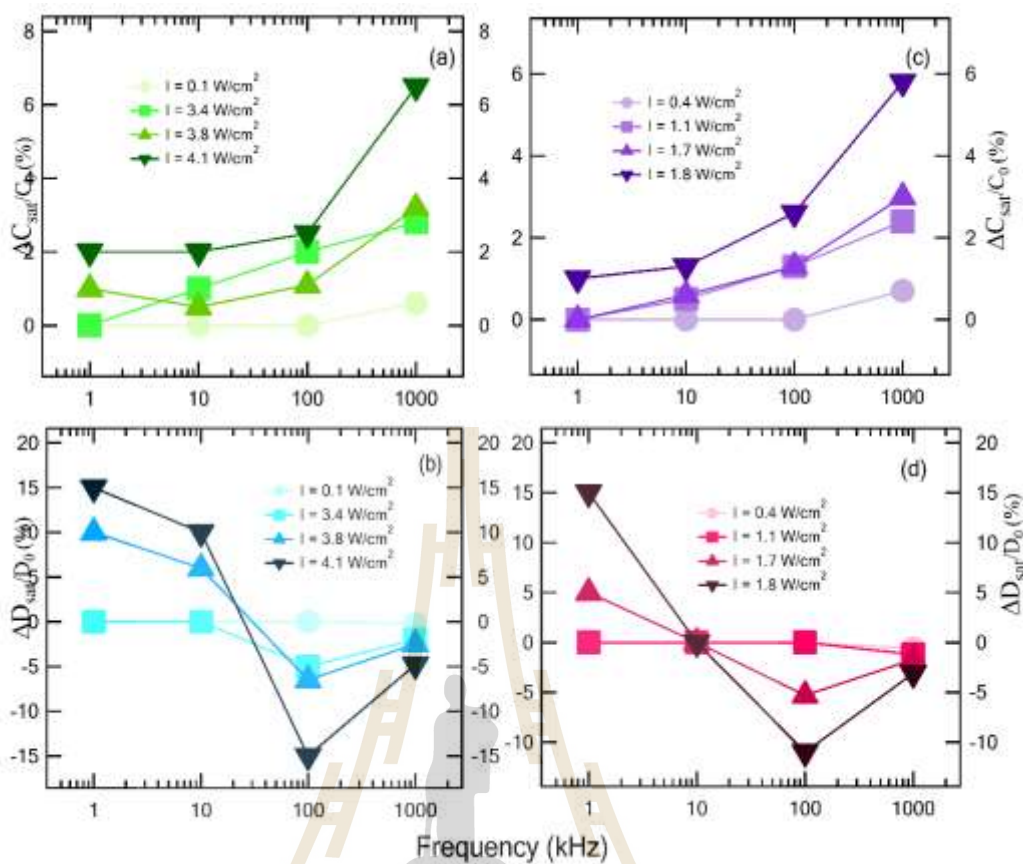


**Figure 4.7** Percentage change of capacitance and loss tangent under of conditions for BBFO-0.3.

#### 4.1.6 BLFO-0.05 ( $\text{Bi}_{0.95}\text{La}_{0.05}\text{FeO}_3$ )

This condition is runner-up for capacitance enhancement under irradiation. Besides being measured by impedance analyzer, this sample was also measured by PES which shows the signature of NEC effect. Trend change of capacitance are same under green and violet irradiations. Then, capacitance can increase more than 10% at 100 kHz of both light. However, the trend for loss tangent is difficult to conclude.

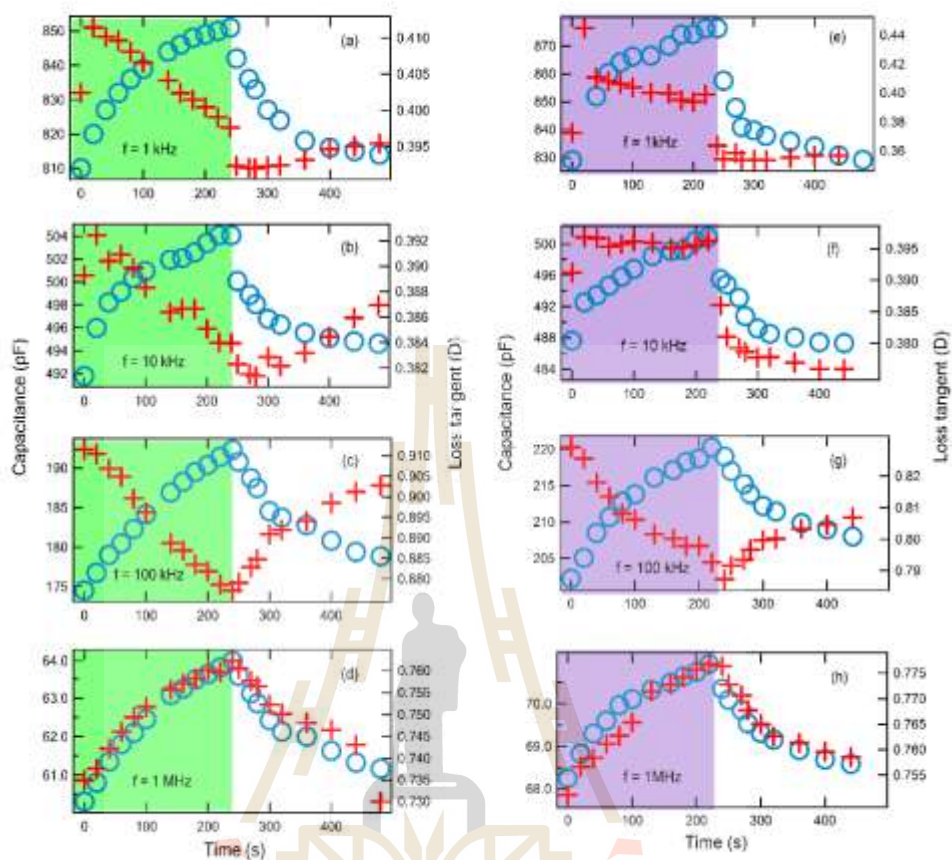


**Figure 4.8** Capacitance and loss tangent of BLFO-0.05 under green irradiation approximate  $4.1 \frac{W}{cm^2}$  (a-d), under violet irradiation approximate  $1.8 \frac{W}{cm^2}$  (e-h).

Percentage change of C, D of all measurement conditions were reported in Figure 4.9. It found that. Capacitance can good response to light at 100 kHz under both irradiations. Loss tangent highest change with light at 1 MHz under green irradiation but highest change at 1 kHz under violet irradiation.

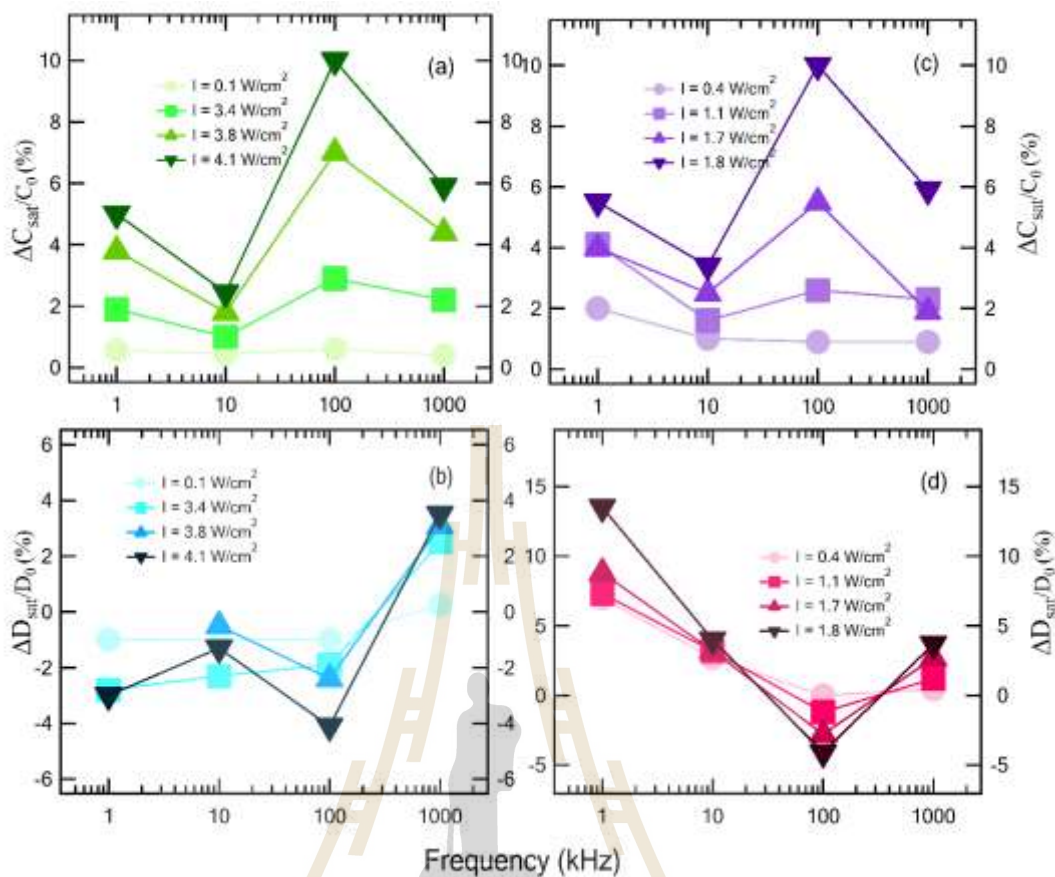


**Figure 4.9** Percentage change of capacitance and loss tangent under of conditions for BLFO-0.05.

#### 4.1.7 BLFO-0.1 ( $\text{Bi}_{0.9}\text{La}_{0.1}\text{FeO}_3$ )

Capacitance of this condition is highest response under irradiation in this research. Capacitance and loss tangent increase up to 12% and 11% at 1 kHz under violet irradiation.

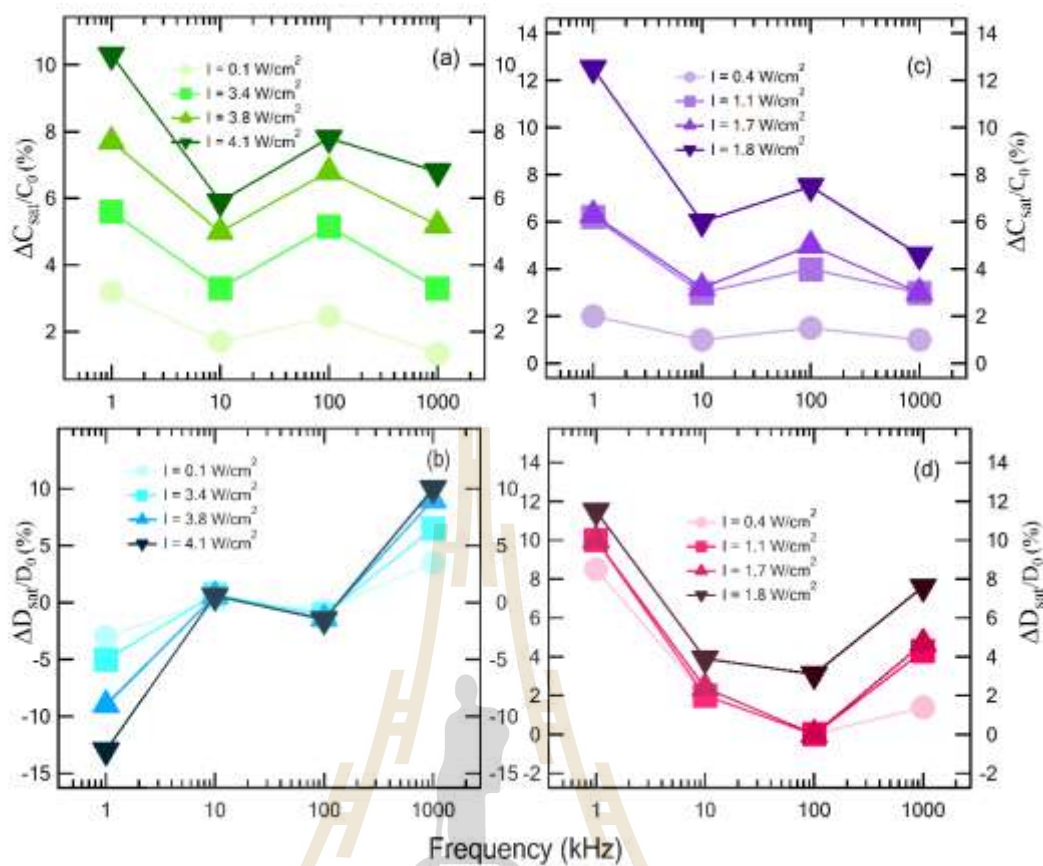


**Figure 4.10** Percentage change of capacitance and loss tangent under of conditions for BLFO-0.1.

#### 4.1.8 BLFO-0.2 ( $\text{Bi}_{0.8}\text{La}_{0.2}\text{FeO}_3$ )

Capacitance of this condition increase about 10% at 100 kHz under both irradiation. Loss tangent increase 15% at 1 MHz under both irradiation as well.

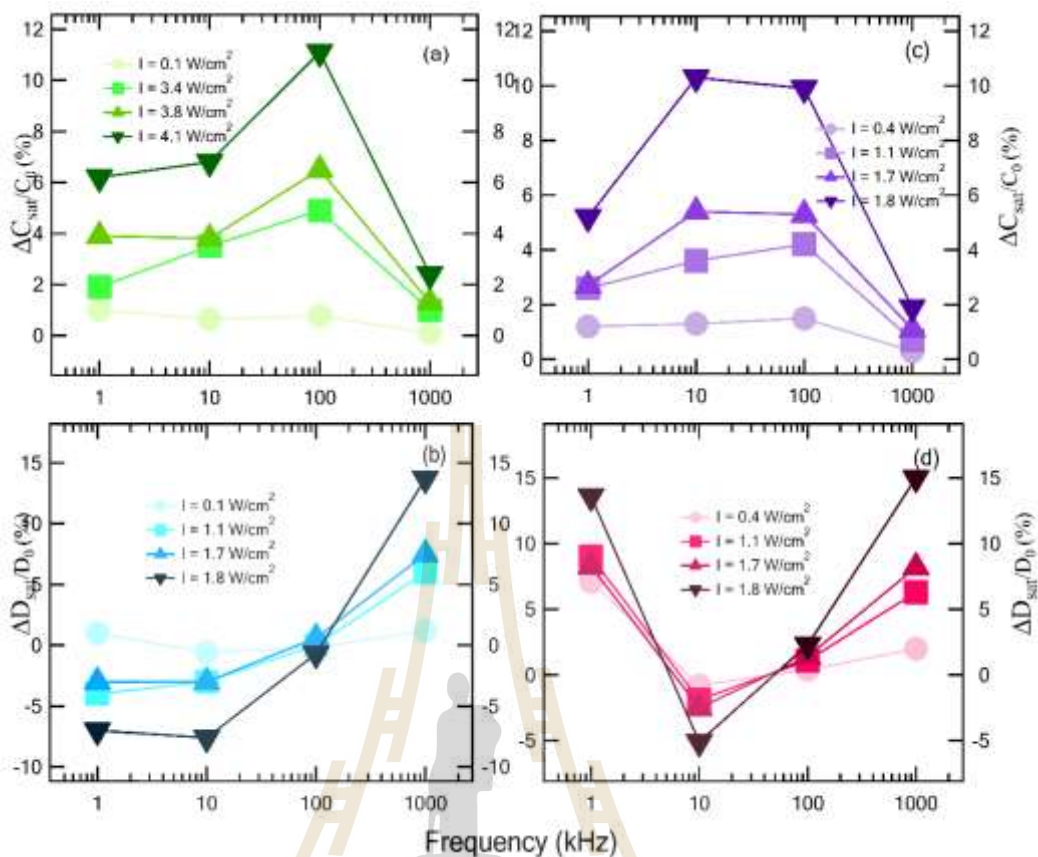


**Figure 4.11** Percentage change of capacitance and loss tangent under of conditions for BLFO-0.2.

#### 4.1.9 BLFO-0.3 ( $\text{Bi}_{0.7}\text{La}_{0.3}\text{FeO}_3$ )

Capacitance increase 11% at 1 kHz under green irradiation, percentage change of capacitance decrease from lower frequency to higher frequency. In contract, percentage change of loss tangent increase with decreasing frequency measurement.

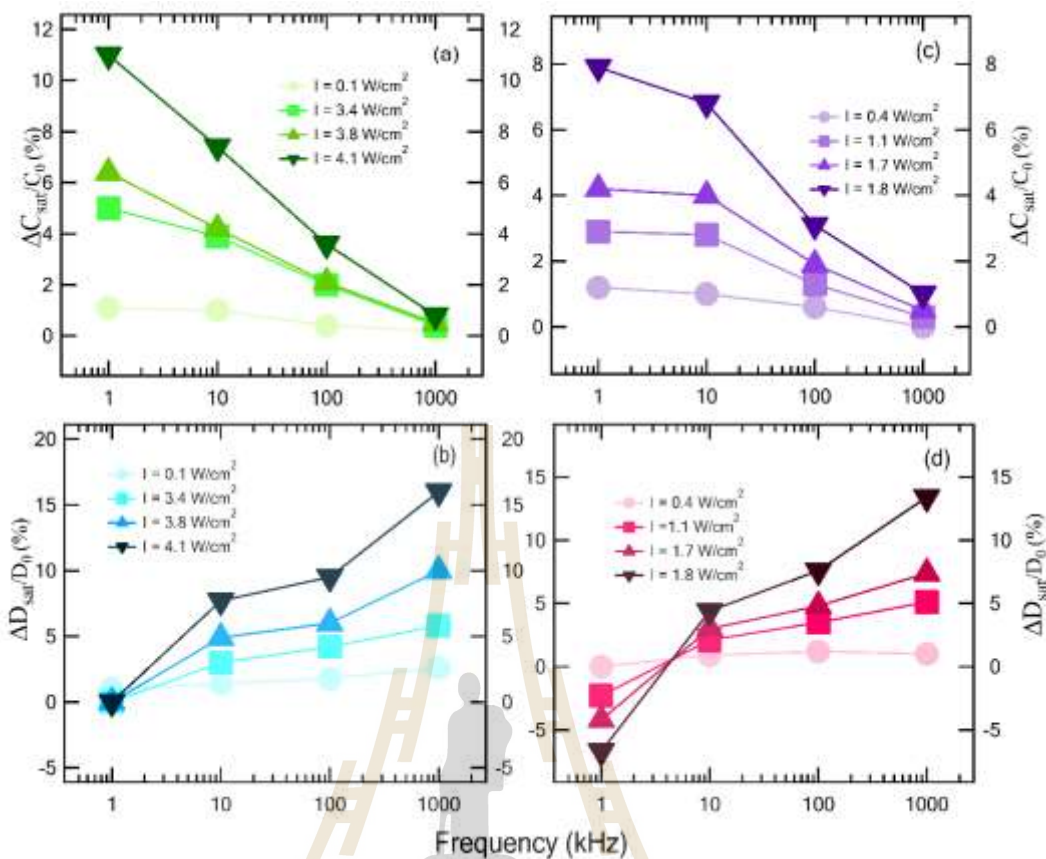


**Figure 4.12** Percentage change of capacitance and loss tangent under of conditions for BLFO-0.3.

To interpret the response of loss tangent with irradiation in this research, we want to reveal some our notice from above results ( $\Delta D_{\text{sat}}/D_0$  (%)). Trend of loss tangent in each condition shows that the slope is different at different frequencies. The slope is positive or negative depending on the frequency. Then, we notice that as shown in Figure 2.8 or 2.9, if slope of loss tangent is positive at a frequency, the loss tangent will decrease under irradiation and vice versa in most cases.

#### 4.1.10 Resistance measurement under irradiation

This measurement was performed to observe any change of resistance (R); this will help confirming if sample becomes more conductive under irradiation. The

electrodes were created on both sides of the top sample surface. And then, light was shined between two electrodes as shown in the inset of Figure 4.13(b). BLFO-0.05 was used for this measurement. At the beginning, resistance value of the sample was about  $100 \text{ M}\Omega$ ; then, this value decreased by 13% and 8% under green about  $4.1 \frac{\text{W}}{\text{cm}^2}$  and violet about  $1.7 \frac{\text{W}}{\text{cm}^2}$  irradiations respectively. In both graphs of Figure 4.13, the resistance decreased (roughly) exponentially under irradiation. This quick response of R in the beginning is similar to the quick response of capacitance, implying the inter-relationship.

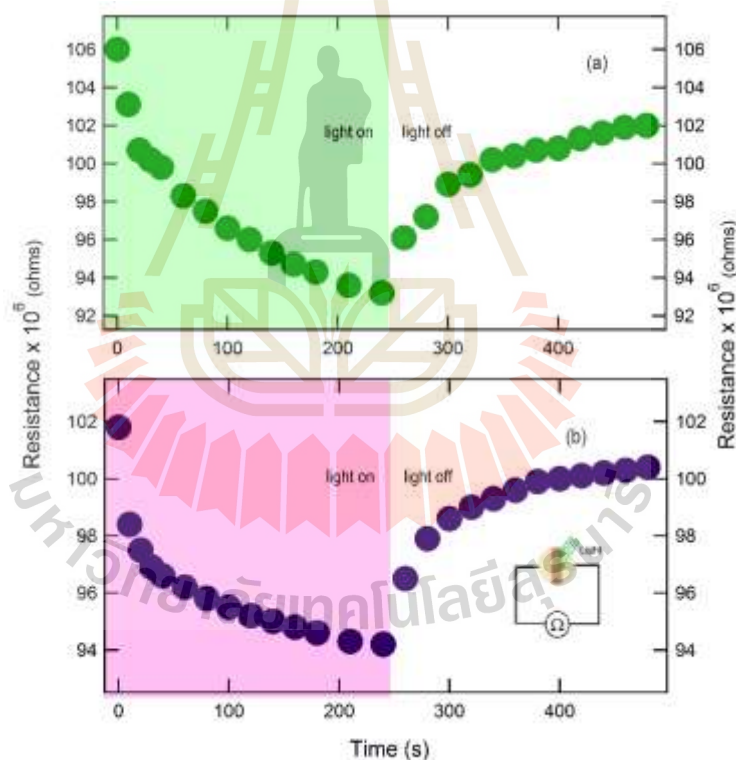


**Figure 4.13** Resistance of BLFO-0.05 under green irradiation about  $4.1 \frac{\text{W}}{\text{cm}^2}$  (a) and under violet irradiation about  $1.7 \frac{\text{W}}{\text{cm}^2}$  (b).

## 4.2 Photoemission measurement and signatures of negative electron compressibility

The following data are experimentally performed at SLRI and ALS. The data were later analyzed in Igor Pro software. These data will help explaining the formation of oxygen vacancy and negative electron compressibility in  $\text{BiFeO}_3$  (thin film), BBFO-0.05 and BLFO-0.05 samples. BBFO-0.05 and BLFO-0.05 were chosen for these measurements because their dielectric constants are highest where  $\text{BiFeO}_3$  will be used as reference. At SLRI, the electronic structures of BBFO-0.05 and BLFO-0.05 samples were measured as shown in Figure 4.13- 4.15. At ALS, the electronic structures of  $\text{BiFeO}_3$ 's thin film and BLFO-0.05 samples were also measured as shown in Figure 4.16- 4.17.

### 4.2.1 $\text{BiFeO}_3$

This photoemission spectroscopy was measured at ALS in USA. Photon energy was set at 50 eV. These spectrum lines showed valence band of thin film  $\text{BiFeO}_3$ ; spectra are colored in black, red, yellow, green, blue, and violet. The exposure time of irradiation is indicated in the figure. The oxygen vacancy state at around 4 eV increases upon increasing irradiation time. The shift of  $\text{O}_{2p}$  state (A region) and oxygen vacancy states (B region) to  $E_F$  is the signature of the negative electron compressibility effect.

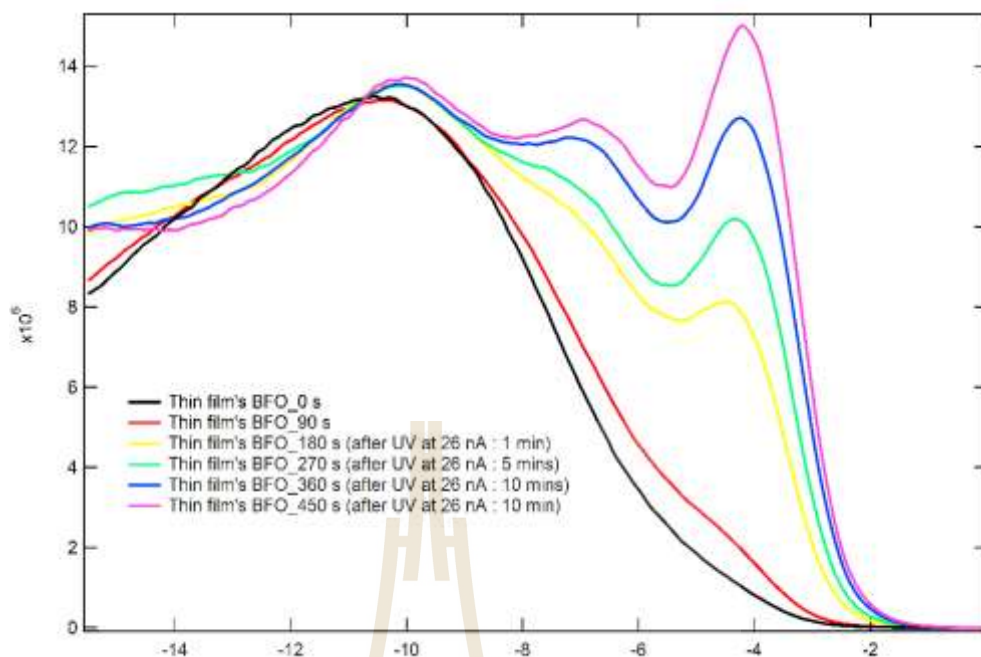


**Figure 4.14** Spectra of valence bands of thin film bismuth ferrite.

#### 4.2.2 BLFO-0.05

In this condition, both oxygen vacancy state and negative electron compressibility were also found under irradiation. PES data of bismuth ferrite doped with 5% lathanum was shown in Figure 4.16. Decreasing of  $O_{2p}$  states at binding energy around 8 eV and increasing of oxygen vacancy states at binding energy around 4 eV were found in electronic structure upon increasing the irradiation time. In this condition, we could detect negative electron compressibility by checking positions of  $O_{2p}$  states which was shifted to Fermi level with increased irradiation time.

Using the analogy of water level in the section 3.3.8, distance between  $C_{1s}$  peak and  $E_f$  is constant, i.e. the distance between bottom of glass to edge of glass. The surface was exposed by light. It means that electrons will be filled (like pouring water into glass). Therefore, If it is natural pheonomena or positive compressibility, then, the energy difference between maximum valence band ( $O_{2p}$  states) and  $E_F$  will be larger

upon filling electrons. We called this positive compressibility. However, in this measurement, maximum valence band ( $O_{2p}$  states) will approach to  $E_F$  upon filling electrons instead.

Quantitatively, maximum valence band was shifted about 0.07 eV after 5 minutes of irradiation time and about 0.15 eV after 30 minutes. To see the shift clearly, we exposed the sample with zeroth order light as shown in Figure 4.16; the energy shift of almost 1.0 eV was observed (see green line). This ensures that BLFO-0.05 exhibits negative electron compressibility effect.

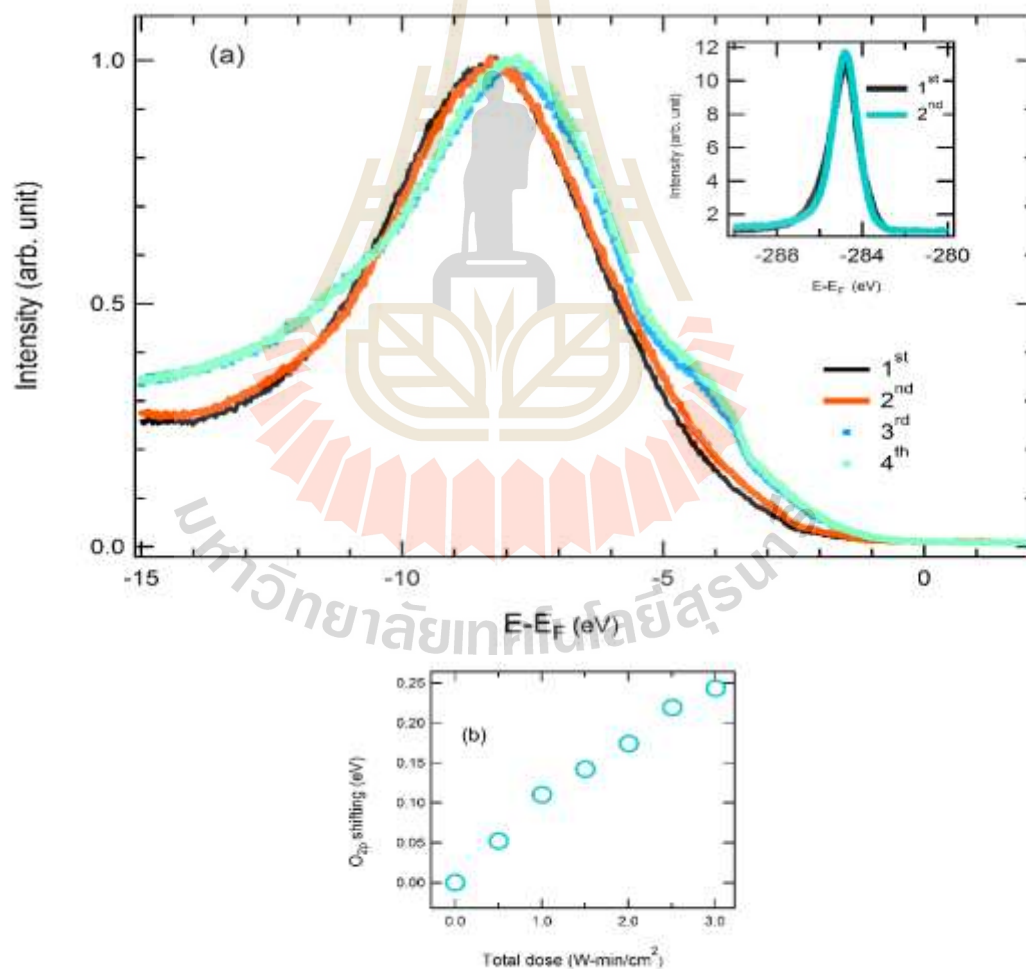


**Figure 4.15** (a) Spectra of valence bands of BLFO-0.05. (b) energy shift of MVB vs irradiation time.

To further ensure the NEC effect, as shown in Figure 4.16, we also measured this sample at ALS which has higher intensity. The change shows similar behavior but at greater magnitude, corresponding to the higher intensity.

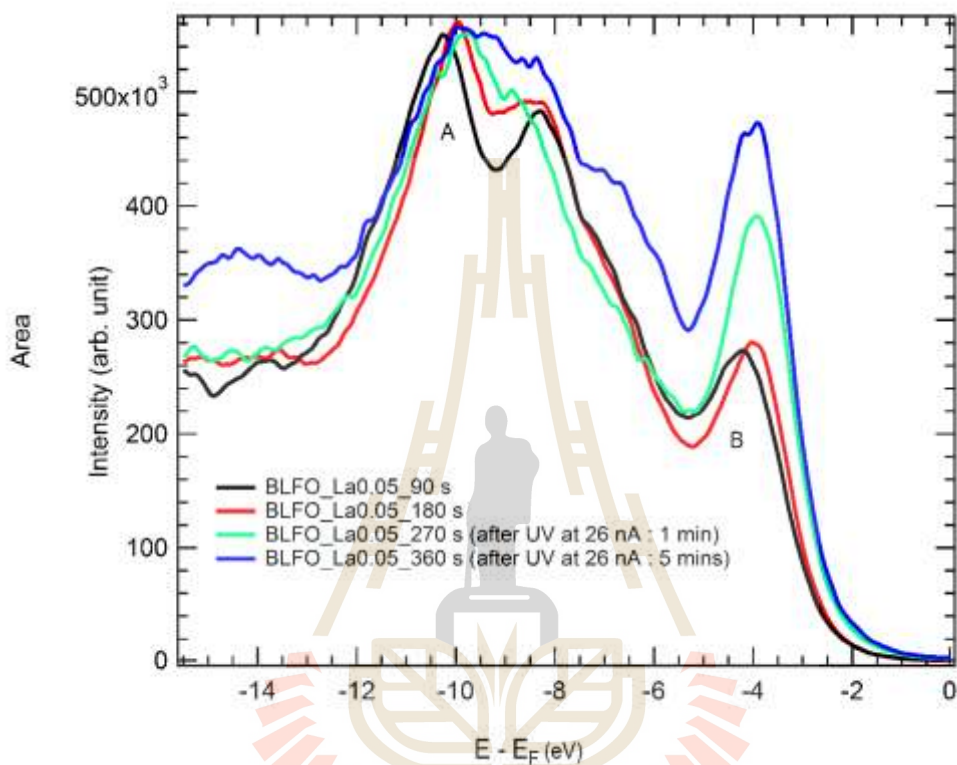


**Figure 4.16** Spectra of valence bands of BLFO-0.05.

### 4.2.3 BBFO-0.05

Photon energy of ultraviolet irradiation was 60 eV and the base pressure was around  $10^{-8}$  torr. Spectra are colored in black, red, yellow, violet and green for BiFeO<sub>3</sub> and BBFO-0.05; each spectrum was collected every 5 minutes. PES data of bismuth ferrite doped with 5% barium was shown in Figure 4.15. Decrease of O<sub>2p</sub> states (region B) and increase of oxygen vacancy states (region C) were observed under irradiation, similar to the BLFO-0.05, suggesting the similar behavior but lesser in degree.

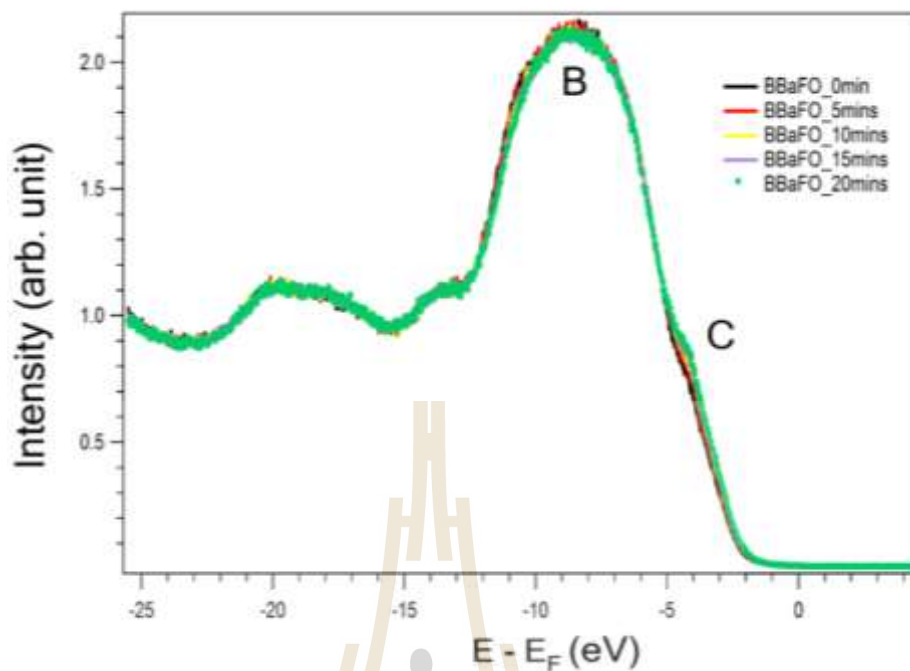


**Figure 4.17** Spectra of valence bands of BBFO-0.05.

### 4.3 Discussions and calculation of capacitance enhanced by the negative electron compressibility effect

From above, capacitance and loss tangent in each condition was measured under irradiation yielding different percentage change. Loss tangent can decrease by 15% in some condition or increase by 60% in another condition. And, the maximum increase in capacitance can be up to 12%. I believe that both properties may find some applications. Resistance of sample was shown to decrease upon increasing irradiation time, indicating that these samples became more conductive under irradiation. This better conductivity corresponds to the change in electronic structure obtained from ARPES which shows the increase of oxygen vacancy state upon increasing the irradiation time. This increase in oxygen vacancy state implies the formation of two-

dimensional electron gas (2DEG) (e.g. Meevasana et al., 2011) which can induce NEC effect (Li et al., 2011).

By using the energy shift of valence band in Figure 4.15, we can calculate the quantum capacitance and then plug it into equation (2) in Chapter II. The details of the calculation is as the following.

Firstly we try to relate the photoemission data and the capacitance measurement by comparing the result of the same irradiation dose which can be calculated from:

$$\text{Dose} = \text{Intensity} \times \text{Time} \quad (11)$$

where intensity of light irradiation has unit which is  $\frac{W}{\text{cm}^2}$  and time of measurement has unit which is minute. Intensity of violet laser light was measured by using optical detector (from ThorLab) to about  $1.8 \frac{W}{\text{cm}^2}$ . In the case that the sample was measured for about 17 seconds, then the dose is  $0.51 \frac{W}{\text{cm}^2} \cdot \text{minutes}$ .

On the other hand, intensity of synchrotron light at SLRI can be calculated from:

$$\text{Intensity} = \left( \frac{\text{No.photon}}{s} \times E_{\text{photon}} \times \left( \frac{1}{A_{\text{beamsize}}} \right) \right) \quad (12)$$

where  $\frac{\text{No.photon}}{s}$  is number of photons per second,  $E_{\text{photon}}$  is energy of photons and  $A_{\text{beamsize}}$  is area of ultraviolet light beam. The number of photons per second was estimated to be about  $3.13 \times 10^{12} \text{ s}^{-1}$ . Energy of photons was set at 60 eV. Area of ultraviolet light beam is expected as equal approximate  $0.3 \times 0.1 \text{ mm}^2$ . Then, intensity of PES measurement is about  $0.1 \frac{W}{\text{cm}^2}$ . Therefore, if the capacitance was measured under violet laser light for 17 seconds, it will take about 5 minutes at SLRI to get the same dose.

After we know the dose in each case, we then try to find  $C_q = Ae^2 \frac{dn}{d\mu}$  where  $d\mu$  is about -0.075 eV from the started spectra and the spectra at 5 minutes ( $d\mu$  is negative because chemical potential shift to lower energy), A is effective area which can be estimated area surface of sample about  $\pi r^2$  (r is about 4.15 mm), e is charge of electron and  $dn = \frac{Q}{e} - 0$  or  $\frac{C_{\text{geometric}}}{e} - 0$  because  $Q = CV = C_{\text{geometric}} \times 1$  (voltage is set at 1 volt), series circuit of capacitor  $Q_{\text{total}} = Q_1 = Q_2 = Q_n$  and surface has no carrier charge in initial state. Therefore, we get  $C_q$  is about  $-1.1 \times 10^{-8}$  F. Then, this value was substituted to equation (2):

$$\frac{1}{C_{\text{total}}} = \frac{1}{C_{\text{geom}}} + \frac{1}{C_q}$$

The calculation is shown in Figure 4.19(b), comparing to the capacitance measured by impedance analyzer (Figure 4.19(a) which is the same data as Figure 4.8(a)). The calculation shows a similar trend of the increase in the same order of magnitude, supporting that NEC effect plays the main role of this capacitance enhancement.

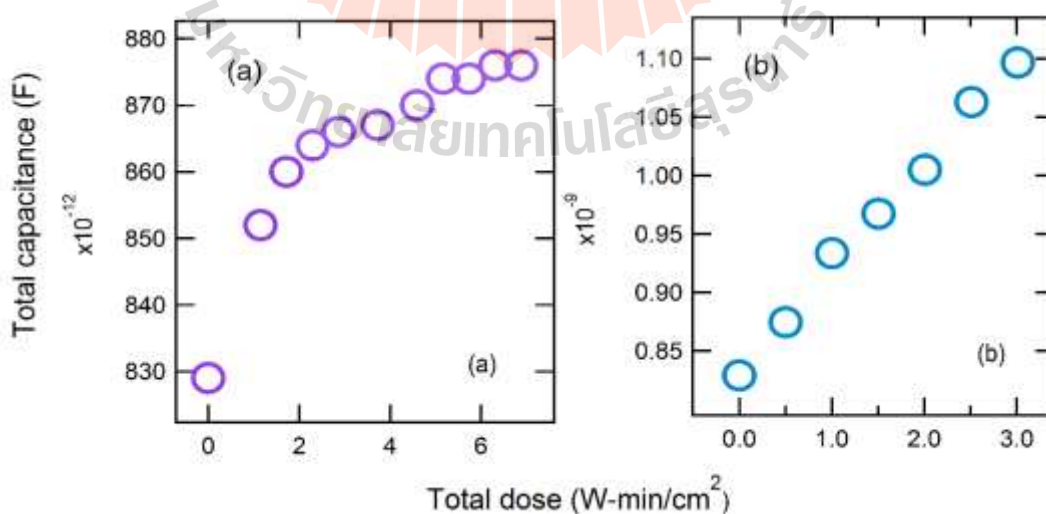


**Figure 4.18** Relationships between  $C_{\text{Total}}$  from real measurement (a),  $C_{\text{Total}}$  from calculation (b) with total dose.

## CHAPTER V

### CONCLUSIONS AND FUTURE RESEARCH

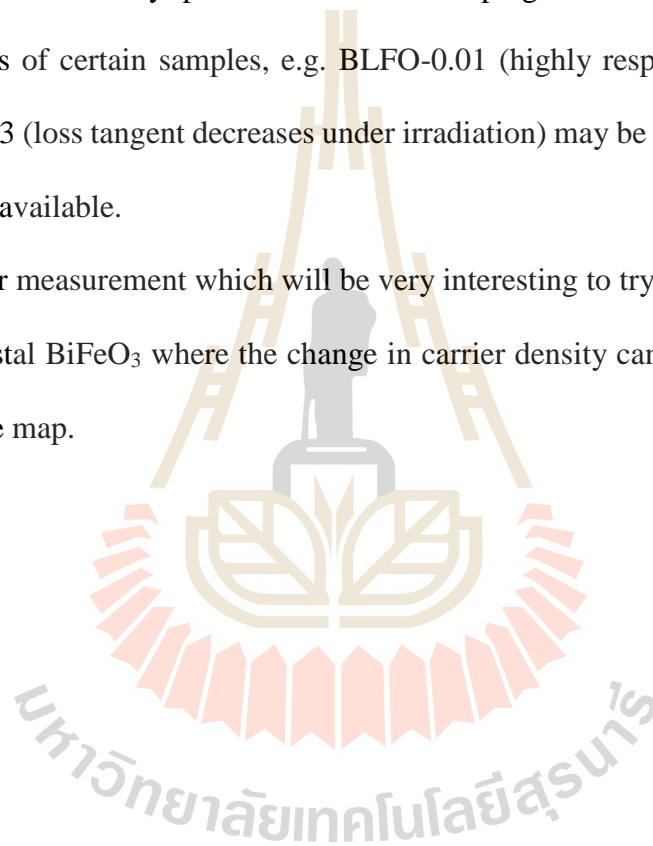
#### 5.1 Conclusions

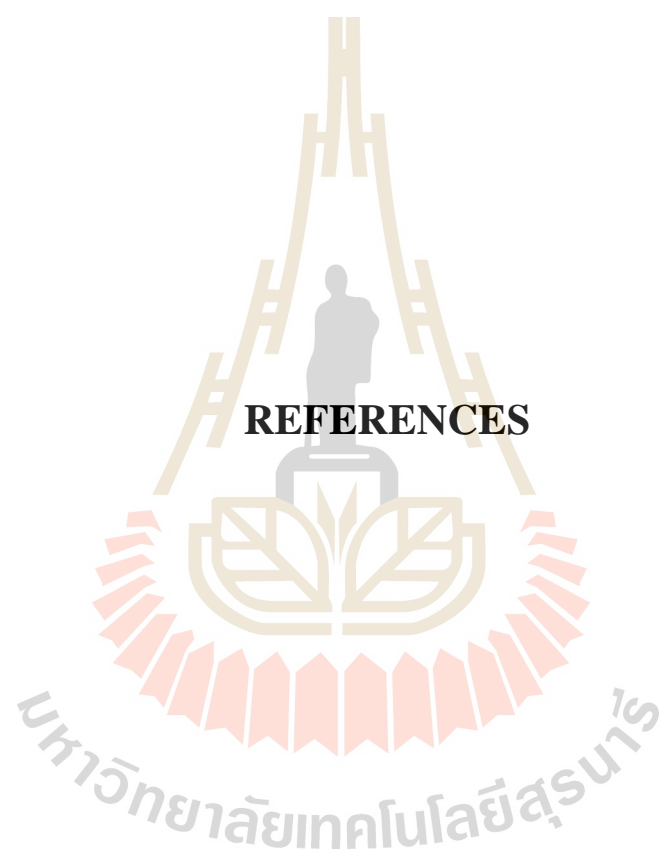
In this work, capacitance measurements under green and violet irradiations were carried out for a series of La-doped and Ba-doped bismuth ferrites (BLFO and BBFO respectively). Maximum percentage change in capacitance is 12% for BLFO-0.2 and maximum change in loss tangent is 65% for BBFO-0.05. In some samples (e.g. BLFO-0.1), loss tangent exhibit was decreased under irradiation. Even though the capacitance enhancement can be caused by various reasons (e.g. photoconductivity and decrease in effective thickness), here, we find that the so-called negative electron compressibility (NEC) effect plays the main role in this enhancement. The enhancement due to this NEC estimated from photoemission data yields a good agreement with the enhancement measured by the impedance analyzer. Note that the NEC effect was confirmed as the chemical potential shift ( $d\mu$ ) (extracted from the energy shift of valence band maximum) was observed to be lower in binding energy after exposing the samples with synchrotron light (UV range), i.e. increasing the carrier density. This negative energy shift effectively creates a capacitor with negative capacitance ( $C_q$ ) which is connected in series with the original (geometric) capacitor and this negative  $C_q$  finally causes the enhancement which can be calculated by using equation (2) in Chapter II).

## 5.2 Improvement/future plan

Regarding the capacitance measured by impedance analyzer, reduction of air gap between surface sample and ITO electrode will help reducing the error. One solution is to directly coat ITO on one side by sputtering technique which will help reducing this air gap. Due to the limitation of measurement time at the synchrotron facilities, PES measurements were only performed on two dopings of the samples. More PES measurements of certain samples, e.g. BLFO-0.01 (highly responsive to violet light) and BBFO-0.3 (loss tangent decreases under irradiation) may be carried out when more beam time is available.

Another measurement which will be very interesting to try is to measure ARPES of single-crystal  $\text{BiFeO}_3$  where the change in carrier density can be obtained from the Fermi surface map.





**REFERENCES**

## REFERENCES

- Agilent Technologies. (2003). **Agilent 4294A Precision Impedance Analyzer Operation Manual (7<sup>th</sup> ed.)**, Japan: Agilent Technologies Japan.
- Aiura, Y., Hase, I., Bando, H., Yasue, T., Saitoh, T., and Dessau, D.S. (2002). Photoemission study of the metallic state of lightly electron doped SrTiO<sub>3</sub>. **Surface Science**. 515: 61-74.
- Basletic, M., Maurice, J.-L., Carretero, C., Herranz, G., Copie, O., Bobes, M., Jacquet, E., Bouzehouane, K., Fusil, S., and Barthelemy, A. (2008). Mapping of the spatial distribution of charge carriers in LaAlO<sub>3</sub>/SrTiO<sub>3</sub> heterostructures. **Nature Materials**. 7: 621-625.
- Basu, S.R., Martin, L.W., Chu, Y.H., Gajek, M., Ramesh, R., Rai, R.C., Xu, X., and Musfeldt, J.L. (2008). Photoconductivity in BiFeO<sub>3</sub> thin films. **Applied Physics Letters**. 92: 091905.
- Choi, T., Lee, S., Choi, Y.J., Kiryukhin, V., and Cheong, S.-W. (2009). Switchable Ferroelectric Diode and photovoltaic effect in BiFeO<sub>3</sub>. **Science**. 324: 63-66.
- Chu, Y.H., Zhao, T., Cruz, M.P., Zhan, Q., Yang, P.L., Martin, L.W., Huijben, M., Yang, C.H., Zavaliche, F., Zheng, H., and Ramesh, R. (2007). Ferroelectric size effects in multiferroic BiFeO<sub>3</sub> thin films. **Applied Physics Letters**. 90: 252906.
- Clark, S.J., and Robertson, J. (2010). Band gap and Schottky barrier heights of multiferroic BiFeO<sub>3</sub>. **Applied Physics Letters**. 90: 132903.

- Dho, J., Qi, X., Kim, H., Judith, L., MacManus-Driscoll, and Mark, G.B. (2006). Large electric polarization and exchange bias in multiferroic BiFeO<sub>3</sub>. **Advanced Materials**. 18: 1445-1448.
- Eisenstein, J.P., Pfeiffer, L.N., and West, K.W. (1991). Negative compressibility of interacting two-dimension electron and quasiparticle gases. **Physical Review Letters**. 68: 674-677.
- Fix, T., Schoofs, F., Macmanus-Driscoll, J.L., and Blamire, M.G. (2009). Charge confinement and Doping at LaAlO<sub>3</sub>/SrTiO<sub>3</sub> interface. **Physical Review Letters**. 103: 166802.
- Gheorghiu, F., Calugaru, M., Ianculescu, A., Musteata, V., and Mitoseriu, L. (2013). Preparation and functional characterization of BiFeO<sub>3</sub> ceramics: A comparative study of the dielectric properties. **Solid State Sciences**. 23: 79-87.
- Godara, P., Agarwal, A., Ahlawat, N., Sanghi, S., and Dahiya, R. (2014). Crystal structure transformation, dielectric and magnetic properties of Ba and Co modified BiFeO<sub>3</sub> multiferroic. **Journal of Alloys and Compounds**. 594: 175-181.
- Godara, P., Agarwal, A., Ahlawat, N., and Sanghi, S. (2015). Crystal structure refinement, dielectric and magnetic properties of Sm modified BiFeO<sub>3</sub> multiferroic. **Journal of Molecular Structure**. 1097: 207-210.
- Hasegawa, T., Mouri, S., Tamada, Y., and Tanaka, K. (2003). Giant photo-induced dielectricity in SrTiO<sub>3</sub>. **Journal of the Physical Society of Japan**. 72: 41-42.
- Henrich, V.E. (1994). The surface science of metal oxides. **New York: Cambridge University Press**. 14-61.
- Hercules, D.M., and Hercules, S.H. Al. (1984). Analytical chemistry of surfaces. Part I General aspects. **Journal of Chemical Education**. 61(5): 402.

- Kemet Corporation. (2014). Measure Capacitance of Class-II and Class-III Ceramic Capacitance (2014). Electronic Component KEMET Corporation.
- King, P.D.C., He, R.H., Eknapakul, T., Buaphet, P., Mo, S.-K., Kaneko, Y., Harashima, S., Hikita, Y., Bahramy, M.S., Bell, C., Hussain, Z., Tokura, Y., Shen, Z.-X., Hwang, H.Y., Baumberger, F., and Meevasana, W. (2012). Subband Structure of a Two-Dimensional Electron Gas Formed at the Polar Surface of the Strong Spin-Orbit Perovskite  $\text{KTaO}_3$ , **Physical Review Letters**. 108: 117602.
- Kumar, A., Rai, R.C., Podraza, N.J., Denev, S., Ramirez, M., Chu, Y.-H., Martin, L.W., Ihlefeld, J., Heeg, T., Schubert, J., Schlom, D.G., Orenstein, J., Ramesh, R., Collins, R.W., Musfeldt, J.L., and Gopalan, V. (2008). Linear and nonlinear optical properties of  $\text{BiFeO}_3$ . **Applied Physics Letters**. 92: 121915.
- Lebeugle, D., Colson, A., and Viret, M. (2007). Very large spontaneous electric polarization in  $\text{BiFeO}_3$  single crystal at room temperature and its evolution under cycling fields. **Applied Physics Letters**. 91: 022907.
- Li, L., Richter, C., Paetel, S., Kopp, T., Mannhart, J., and Ashoori, R.C. (2011). Large capacitance enhancement and negative compressibility of two-dimensional electronic systems at  $\text{LaAlO}_3/\text{SrTiO}_3$  interfaces. **Science**. 332: 825.
- Liu, J., Li, M.Y., Pei, L., Yu, B.F., Guo, D.Y., and Zhao, X.Z. (2009). Effect of Ce doping on the microstructure and electrical properties of  $\text{BiFeO}_3$  thin films prepared by chemical solution deposition. **Journal of Physics D: Applied Physics**. 42: 115409.
- Masingboon, C., Eknapakul, T., Suwanwong, S., Buaphet, P., Nakajima, H., Mo, S.-K., Thongbai, P., King, P.D.C., Maensiri, S., and Meevasana, M. (2013). Anomalous

change in dielectric constant of  $\text{CaCu}_3\text{Ti}_4\text{O}_{12}$  under violet-to- ultraviolet irradiation. **Applied Physics Letters**. 102: 202903.

Mazumder, R., Sujatha Devi, P., Bhattacharya, D., Choudhury, P., Sen, A., and Raja, M. (2007). Ferromagnetism in nanoscale  $\text{BiFeO}_3$ . **Applied Physics Letters**. 91: 062510.

Meevasana, W., King, P.D.C., He, R.H., Mo, S.-K., Hashimoto, M., Tamai, A., Songsiriritthigul, P., Baumberger, F., and Shen, Z.-X. (2011). Creation and control of a two-dimensional electron liquid at the bare  $\text{SrTiO}_3$  surface. **Nature Materials**. 10: 114.

Meevasana, W., Zhou, X.J., Moritz, B., Chen, C.-C., He, R.H., Fujimori, S.-I., Lu, D.H., Mo, S.-K., Moore, R.G., Baumberger, F., Devereaux, T.P., Marel van der, D., Nagaosa, N., Zaanen, J., and Shen, Z.-X. (2010). Strong energy-momentum dispersion of phonon-dressed carriers in the lightly doped band insulator  $\text{SrTiO}_3$ . **New Journal of Physics**. 12: 023004.

Neaton, J.B., Ederer, C., Waghmare, U.V., Spaldin, N.A., and Rabe, K.M. (2005). First-principles study of spontaneous polarization in multiferroic  $\text{BiFeO}_3$ . **Physical Review B**. 71: 014113.

Putjuso, T. (2012). Giant Dielectric Materials. **KKU Science**. 40(1): 54-65.

Riley, J.M., Meevasana, W., Bawden, L., Asakawa, M., Takayama, T., Eknapakul, T., Kim, T.K., Hoesch, M., Mo, S.-K., Takagi, H., Sasagawa, T., Bahramy, M.S., and King, P.D.C. (2015). Negative electron compressibility and tunable spin splitting in  $\text{WSe}_2$ . **Nature Nanotechnology**. 217: 1043-1047.

Santander-Syro, A.F., Copie, O., Kondo, T., Fortuna, F., Pailhes, S., Weht, R., Qiu, X.G., Bertran, F., Nicolaou, A., Taleb-Ibrahimi, A., Le Fevre, P., Herranz, G.,

- Bibes. M., Reyren. N., Apertet. Y., Lecoœur. P., Barthelemy. A., and Rozenberg. M.J. (2010). Two-dimensional electron gas with universal subband at the surface of SrTiO<sub>3</sub>. **Nature**. 469: 189-193.
- Sing, M., Berner, G., Goss, K., Muller, A., Ruff, A., Wetscherek, A., Thiel, S., Mannhart, J., Pauli, S.A., Schineider, C.W., Willmott, P.R., Gorgoi, M., Schafers, F., and Claessen, R. (2009). Profiling the interface electron gas of LaAlO<sub>3</sub>/SrTiO<sub>3</sub> heterostructures with hard x-ray photoemission spectroscopy. **Physical Review Letters**. 102: 176805.
- Singh, P., and Jung, J.H. (2010). Effect of oxygen annealing on magnetic, electric and magnetodielectric properties of Ba-doped BiFeO<sub>3</sub>. **Physica B**. 405: 1086-1089.
- Takesada, M., Yagi, T., Itoh, M., and Koshihara, S.A. (2003). gigantic photoinduced dielectric constant of quantum paraelectric perovskite oxides observed under a weak DC electric field. **Journal of the Physical Society of Japan**. 72: 37-40.
- Tanaka, I., Oba, I., Tatsumi, K., Kunisu, M., Nakano, M., and Adachi, H. (2002). Theoretical Formation Energy of Oxygen-Vacancies in Oxides. **Materials Transactions**. 43(7): 1426-1429.
- Waldrip, M., and Tse, R. (2000). **Capacitance Measurement Tips for High Capacitance MLCC's, 2000**: TDK component USA, Inc.
- Wang, J., Neaton, J.B., Zheng, H., Nagarajan, V., Ogale, S.B., Liu, B., Viehland, D., Vaithyanathan, V., Schlom, D.G., Waghmare, U.V., Spaldin, N.A., Rabe, K.M., Wuttig, M., and Ramesh, R. (2003). Epitaxial BiFeO<sub>3</sub> multiferroic thin film heterostructures. **Science**. 299: 1719-1721.

- Wang, Y.P., Zhou, L., Zhang, M.F., Chen, X.Y., Liu, J.-M., and Liu, Z.G. (2004). Room-temperature saturated ferroelectric polarization in BiFeO<sub>3</sub> ceramics synthesized by rapid liquid phase sintering. **Applied Physics Letters**. 84: 1731.
- Xu, J.P., Zhang, R.J., Chen, Z.H., Wang, Z.Y., Zhang, F., Yu, X., Jiang, A.Q., Zheng, Y.X., Wang, S.Y., and Chen, L.Y. (2014). Optical properties of epitaxial BiFeO<sub>3</sub> thin film grown on SrDuO<sub>3</sub>-buffered SrTiO<sub>3</sub> substrate. **Nanoscale Research Letters**. 9(1): 188.
- Yotburut, B., Yamwong, T., Thongbai, P., and Meansiri, S. (2014). Synthesis and characterization of coprecipitation-prepared La-doped BiFeO<sub>3</sub> nanopowders and their bulk dielectric properties. **Japanese Journal of Applied Physics**. 53: 06JG13.
- Zelezny, V., Chvostova, D., Pajasova, L., Vrejolu, I., and Alexe, M. (2010). Optical properties of epitaxial BiFeO<sub>3</sub> thin films. **Applied Physics A**. 100: 1217-1220.
- Zhang, X., Zhao, L., Fan, C., Liang, Z., and Han, P. (2012). Effects of oxygen vacancy on the electronic structure and absorption spectra of bismuth oxychloride. **Computational Materials Science**. 61: 180-184.

## CURRICULUM VITAE

Name: Mr. Sarawudh Nathabumroong

Date of birth: 17 January 1991

Place of birth: Yasothon, Thailand

Nationality: Thai

### Education

Academic year

2009-2012 Khon kaen University, Khon kaen, Thailand.

Bachelor of Science (Physics)

2013-2016 Suranaree University of Technology, Nakhon Ratchasima,  
Thailand.

Master of Science (Physics)

มหาวิทยาลัยเทคโนโลยีสุรนารี